Small

NANO · MICRO small
www.small-journal.com

REVIEW

Editor's Choice

Recent Advances in Lithium Metal Anodes with Liquid Electrolytes: Interfacial Interaction-Driven Assembly for Dendrite Suppression and Long-Term Stability

Chanseok Lee[1] | Boyeon Kim[1] | Hyunjun Hwang[2] | Jun Hyuk Moon[1] | Yoon Jang Chung[1] | Hyeong Jun Kim[3] | Yongmin Ko[4] | Jinhan Cho[1,2,5]

[1]Department of Chemical & Biological Engineering, Korea University, Seoul, Republic of Korea | [2]KU-KIST Graduate School of Converging Science and Technology, Korea University, Seoul, Republic of Korea | [3]Department of Chemical and Biomolecular Engineering, Sogang University, Seoul, Republic of Korea | [4]Division of Energy & Environmental Technology, Materials Research Institute, Daegu Gyeongbuk Institute of Science and Technology (DGIST), Daegu, Republic of Korea | [5]Soft Hybrid Materials Research Center, Korea Institute of Science and Technology (KIST), Seoul, Republic of Korea

Correspondence: Yongmin Ko (yongmin.ko@dgist.ac.kr) | Jinhan Cho (jinhan71@korea.ac.kr)

Received: 28 October 2025 | **Revised:** 5 January 2026 | **Accepted:** 21 January 2026

Keywords: interfacial interaction | li dendrite growth | li metal anode | separator

ABSTRACT

The direct use of lithium (Li) metal as an anode provides a promising route toward next-generation batteries with ultrahigh energy density. However, its practical realization remains severely constrained by safety and stability issues arising from uncontrolled Li dendrite growth and unstable solid–electrolyte interphases. To overcome these challenges, various strategies have been developed, including the construction of artificial interphases, lithiophilic surface modification of current collectors or separators, and the fabrication of 3D porous current collectors. These approaches are primarily designed to mitigate Li-ion concentration polarization and homogenize interfacial energy distribution, thereby suppressing dendritic deposition. Conventional methods, however, often rely on slurry coating of lithiophilic materials, which introduces inactive binders and thick layers. In contrast, layer-by-layer (LbL) assembly driven by interfacial interactions has recently emerged as a powerful alternative, enabling molecular-level control over film composition and architecture. This strategy allows the formation of ultrathin and binder-free coatings that simultaneously enhance electronic conductivity, electrochemical stability, and energy density. This perspective reviews recent advances in the fabrication of high-performance Li metal anodes and demonstrates how interfacial interaction–mediated LbL assembly can serve as a transformative approach for realizing dendrite-free, durable Li metal anodes and high-energy-density batteries with superior interfacial and cycling stability.

1 | Introduction

The rapidly growing demand for high-energy-density rechargeable batteries in electric vehicles, grid-scale energy storage, and portable electronics has accelerated the exploration of advanced electrode materials that surpass conventional graphite-based technologies. Among the various candidates, Li metal stands out as the most promising anode material due to its exceptionally high theoretical specific capacity (3860 mAh g^{-1}), the lowest redox potential (−3.04 V vs. SHE), and ultralow density (0.534 g cm^{-3}) [1, 2]. These intrinsic properties make Li metal anodes highly attractive for constructing next-generation batteries with

Chanseok Lee, Boyeon Kim, and Hyunjun Hwang. contributed equally to this work.

significantly enhanced energy density when paired with high-capacity cathodes such as sulfur, oxygen, or high-nickel layered oxides. Consequently, Li–sulfur (Li—S), Li–air (Li—O_2), and anode-free Li metal batteries (LMBs) have emerged as promising platforms with the potential to revolutionize electrochemical energy storage technologies [3, 4].

However, despite these advantages, the practical application of Li metal anodes (LMAs) remains elusive due to a series of persistent and interrelated challenges. The most critical issue is the uncontrolled growth of Li dendrites during repeated Li plating and stripping, which stems from the nonuniform deposition of Li^+ ions at the electrode/electrolyte interface [5]. These needle-like dendritic structures not only lead to low Coulombic efficiency through continuous Li consumption but also pose a serious safety hazard by causing internal short circuits. Moreover, the high chemical reactivity of Li metal with conventional organic liquid electrolytes triggers the continuous formation and breakdown of the solid electrolyte interphase (SEI)—an intrinsically unstable and heterogeneous layer that accelerates electrolyte depletion and impedes Li-ion transport [6, 7]. In addition, the substantial volume fluctuations (>100%) of Li metal during cycling generates severe mechanical stress, delamination, and poor interfacial contact, ultimately resulting in rapid capacity degradation and limited cycling reversibility [8, 9].

To overcome these challenges, numerous strategies have been proposed to regulate interfacial reactions and promote uniform Li deposition, including host electrode modification [10, 11], separator functionalization [12, 13], and electrolyte optimization [14–17]. For example, conductive and lithiophilic species—materials or functional groups possessing a strong affinity for Li—have been incorporated to reduce the nucleation overpotentials, guide the homogeneous Li deposition, and buffer volume changes. Functional separators modified by lithiophilic components have also been designed to regulate ionic flux and suppress dendrite growth, while electrolyte compositions have been optimized to promote the formation of robust and inorganic-rich SEI layers. Although these approaches have yielded significant improvements in electrochemical performance, most modifications—particularly those applied to host electrodes and separators— still rely heavily on conventional slurry-coating processes that entail several inherent limitations. These include poor control over coating thickness and uniformity, uneven distribution of active components, limited conformality on complex 3D structures, and the inclusion of inactive binders or additives that can dilute electrochemical activity. Moreover, the incorporation of insulating polymer binders within thick slurry layers (ranging from a few to several tens of micrometers) can significantly reduce porosity and hinder charge transport, thereby diminishing the overall performance gains. In particular, the large thickness or high mass loading of slurry-based interlayers also leads to a marked reduction in the energy density of LMBs. Consequently, researchers and battery manufacturers are increasingly pursuing ultrathin, highly lithiophilic interlayers on host electrodes or separators—objectives that remain difficult to realize through slurry casting. As a result, the performance improvements achieved via slurry-based strategies often fall short of meeting the requirements for long-term, high-performance operation in practical LMBs.

As a promising alternative to conventional slurry-based approaches, solution-processable, interfacial interaction-driven assembly techniques have recently emerged as effective strategies to overcome the structural and compositional limitations of LMAs. In contrast to traditional methods that produce thick, inhomogeneous coatings containing inactive binders or additives, these assembly-based techniques enable the precise and uniform deposition of ultrathin interfacial layers directly onto a wide range of substrates—including porous, flexible, or geometrically complex current collectors—without the need for slurry processing. By harnessing well-defined intermolecular interactions such as electrostatic attraction, hydrogen-bonding, and covalent-bonding interactions, these methods provide molecular-level control over the interfacial architecture. This high degree of tunability not only ensures conformal and compositionally uniform surface coatings but also promotes homogeneous Li^+ ion flux, the formation of stable, inorganic-rich SEI layers, and effectively suppresses dendritic Li growth during repeated cycling.

Furthermore, because the formation of ultrathin (<100 nm) lithiophilic interlayers on host electrodes or separators is critical for achieving high energy-density LMBs, it is highly desirable to construct such interlayers without polymeric binders, which diminish electrochemical activity and increase the overall thickness or mass. The additive-free nature and structural precision of solution-processable, interfacial assembly techniques therefore confer distinct advantages in terms of electrochemical performance, mechanical stability, and process scalability—key attributes for next-generation LMB technologies. Moreover, their inherent compatibility with diverse substrate geometries and large-area fabrication further highlights their potential for industrial-scale implementation.

In this perspective, we present a comprehensive review of recent progress in LMAs operating in liquid electrolyte environments, with a particular emphasis on strategies driven by interfacial interactions (Scheme 1). We first elucidate the fundamental degradation mechanisms of LMAs—including unstable SEI formation, dendritic Li growth, and poor interfacial contact—before summarizing current advancements in host electrode design, separator functionalization, and electrolyte optimization. Subsequently, we spotlight emerging interfacial assembly approaches that harness molecular-level design principles to construct ultrathin, lithiophilic, and functionally active coatings. These strategies are shown to surpass conventional slurry-based coatings in terms of structural precision, functional integration, and long-term stability. Finally, we address the remaining challenges—such as scalable fabrication, advanced interfacial characterization, and seamless integration into commercial cell architectures—and propose future research directions toward practical and reliable Li metal battery systems. By clarifying the central role of interfacial interactions in governing Li deposition and electrode stability, this perspective aims to guide the rational design and scalable realization of next-generation interfacial architectures for safe, reversible, and high-performance LMAs.

In contrast to prior review articles that primarily categorize interfacial engineering strategies based on material compositions, structural motifs, or geometric parameters—and subsequently correlate these characteristics with LMA performance

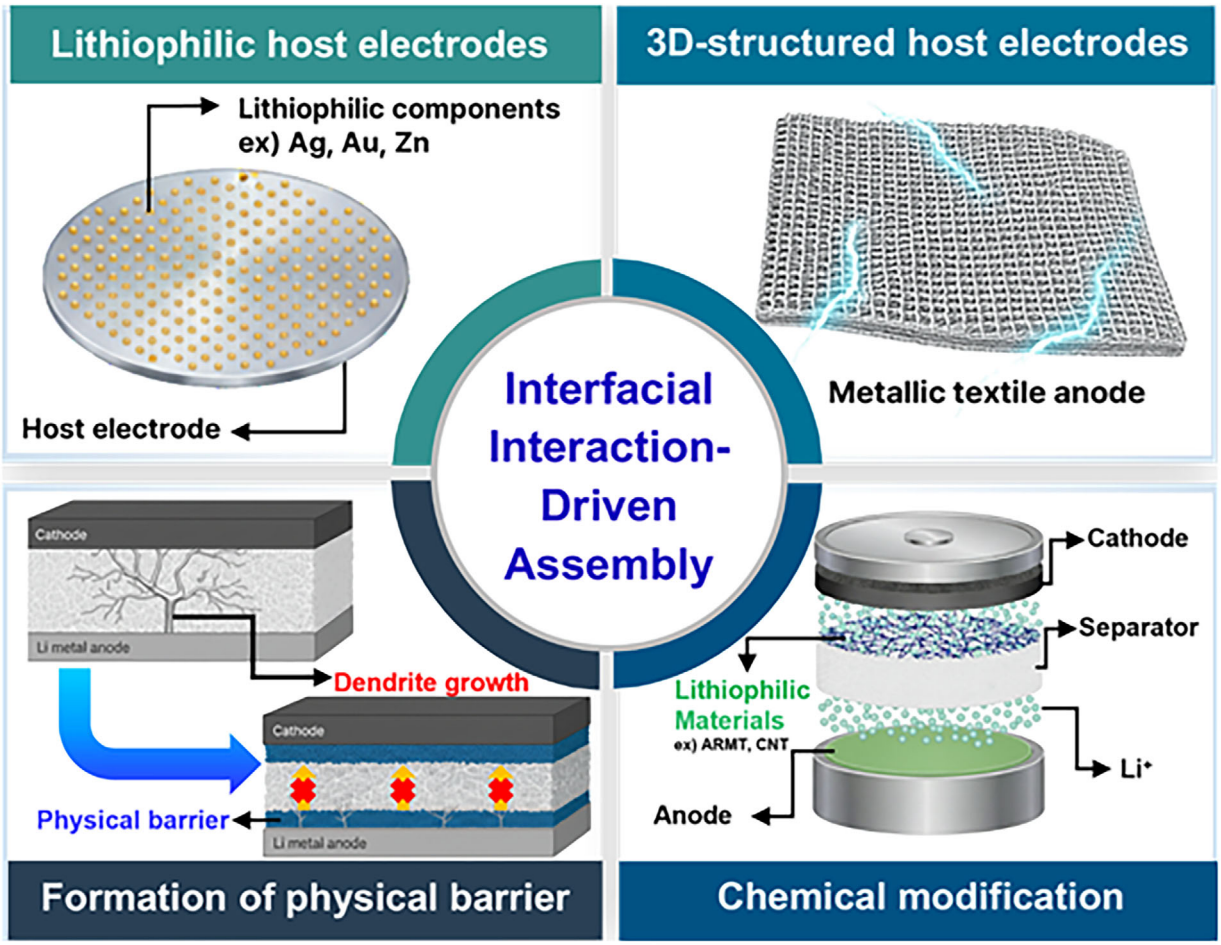

SCHEME 1 | Schematic illustration of interfacial interaction-driven assembly-enabled electrode and separator strategies for LMAs.

metrics [18–20], this Perspective introduces a fundamentally different conceptual framework by positioning interfacial interactions among all electrode components as the central and unifying design variable. Rather than viewing interfaces as static boundaries defined solely by material identity or morphology, we emphasize that the nature of interfacial interactions and the interaction-induced functional groups across electrode interfaces ultimately govern interfacial formation, lithiophilic behavior, and the resulting electrochemical performance of LMAs.

Importantly, this interaction-centric perspective enables a more rigorous and mechanistic interrogation of charge-transport kinetics at nanoscale interfaces, where ion and electron transfer processes are intrinsically coupled to local chemical environments. By contrast, in conventional slurry-cast functional interlayers, such interfacial effects are often masked—or even entirely inaccessible—owing to micrometer-scale thicknesses, heterogeneous component distributions, and phase segregation, which cause electrochemical behavior to be dominated by bulk transport rather than interfacial processes.

Within this framework, we systematically analyze how both the type and strength of interfacial interactions—spanning electrostatic interactions, hydrogen bonding, and covalent coupling—collectively dictate key interfacial attributes, including interlayer cohesion, ion/electron transport continuity, and long-term electrochemical stability. By explicitly connecting molecular-scale interactions to rationally designed interfacial architectures, this Perspective provides a coherent and generalizable blueprint for engineering solution-processable, ultrathin, and binder-free interlayers with unprecedented molecular-level precision.

In this context, the term "molecular-level design" denotes a deliberate and quantitative engineering of interfacial characteristics at the scale of individual chemical interactions. This includes: i) precise control over the identity, spatial distribution, and surface density of functional groups—such as polar or charged functional groups and specific coordination sites; ii) modulation of the local electrostatic and chemical environment that governs Li^+ adsorption, desolvation, and interfacial accumulation; and iii) rational tuning of the interfacial energy profile that ultimately determines the nucleation overpotential and nucleation pathway of metallic Li.

For instance, functional groups incorporating the specific interactions within the functional interlayers, such as $-SO_3H$, $-COOH$, $-OH$, and $-NH_2$, can influence ion adsorption behavior and the concentration gradient at the interface, creating a localized electrostatic field that attracts Li^+ ions from the bulk electrolyte [21–23]. Furthermore, these polar groups within the formed lithiophilic interlayers can interact strongly with carbonate solvent molecules (e.g., ethylene carbonate, EC)

through hydrogen-bond and dipole-dipole interactions [24, 25], thereby partially competing with Li^+ for solvent coordination near the interface. This competitive interaction locally perturbs the Li^+ solvation structure, weakens Li^+–solvent binding, and facilitates interfacial desolvation and homogeneous Li^+ flux. Therefore, by systematically regulating these interrelated parameters, interaction-engineered interfaces can effectively homogenize Li^+ flux at the electrode surface, facilitate the formation of mechanically robust and inorganic-rich SEIs, and direct Li deposition away from stochastic, dendritic growth toward dense, uniform, and morphologically stable deposits.

2 | Li Dendrite Formation and Growth in Li Metal Anodes

The formation of Li dendrites in LMAs arises from the intricate interplay among nonuniform Li nucleation, ionic transport limitations, interfacial chemistry, and mechanical instability. During the initial plating process, Li tends to deposit preferentially at sites with lower nucleation barriers—determined by the lithiophilicity, surface morphology, and compositional uniformity of the current collector or the pre-existing Li surface. In practical operation, an LMA experiences repeated cycles of Li plating during charging and stripping during discharging. Throughout the plating process, Li^+ ions are chemically reduced at the electrode surface to form initial nuclei, which progressively grow into dendritic structures (Figure 1a) [26]. With continuous cycling, these needle-like dendrites extend further, degrading the battery's lifespan, efficiency, and safety [27, 28]. Therefore, preventing dendrite formation and achieving safe, long-lasting operation requires electrode designs that ensure uniform current density and homogeneous ion distribution across the LMA surface. In the following section, we discuss in detail the key factors governing the nucleation and growth of Li dendrites.

2.1 | Formation and Growth Mechanism of Li Dendrites

Modeling studies have revealed a pronounced difference between the electrical potentials at the dendrite base (φ_s) and tip (φ_t), with φ_t increasing as the principal radius of curvature decreases [29, 30]. Accordingly, sharper dendrite tips exhibit higher tip potentials. These tips also feature a high density of atomic steps and kinks, which enhances the exchange current density for Li deposition. As a result, the activation energy and overpotential for Li plating at the tip become significantly lower than those on flat surface regions, promoting preferential deposition and directional growth along the protrusion. The resulting potential difference ($\Delta\varphi = \varphi_t - \varphi_s$), therefore, serves as an intrinsic driving force for dendrite propagation. Moreover, the reduced overpotential at the tip further accelerates anisotropic growth toward the electrolyte, amplifying the instability of the electrode surface. (Figure 1b) [31].

Ely et al. developed a unified framework to rationalize the nucleation and growth of Li electrodeposits by integrating thermodynamic and kinetic principles (Figure 1c) [32, 33]. In this model, electrodeposition proceeds only when an initial Li embryo surpasses both a critical thermodynamic radius—beyond which dendrite formation becomes energetically favorable—and a critical kinetic radius—required for continuous growth. Based on these criteria, several behavioral regimes were proposed to describe the evolution of electrodeposits. In the nucleation suppression regime, embryos remain thermodynamically unstable and readily redissolve into the electrolyte. Under small overpotentials corresponding to the long-incubation-time regime, nuclei with sizes between the two critical radii can gradually grow. In contrast, at large overpotentials within the short-incubation-time regime, rapid nucleation yields numerous small, nearly monodisperse nuclei. During the early growth regime, nuclei that satisfy both thermodynamic and kinetic requirements grow steadily; however, in the late growth regime, morphological instabilities and localized electric-field intensification dominate, giving rise to dendritic structures. Consistent with this framework, Aniruddha et al. formulated a thermodynamically consistent growth theory based on the Gibbs–Duhem relation, demonstrating that high interfacial energy and a low Gibbs free energy of transformation can effectively delay dendrite initiation [34]. They further demonstrated that dendrite formation can be avoided by selecting appropriate overpotentials and anode particle sizes to operate within the thermodynamic suppression regime.

Therefore, surfaces with poor lithiophilicity or chemical heterogeneity aggravate dendritic growth by inducing sparse nucleation, which concentrates current on a limited number of active sites and leads to needle-like Li deposits. As cycling continues, ionic transport limitations become increasingly dominant. Under galvanostatic conditions, the consumption rate of Li^+ at the electrode–electrolyte interface may exceed its replenishment, particularly at high current densities, low electrolyte concentrations, low Li^+ diffusivity, or when the Li^+ ion transference number is small. This imbalance gives rise to severe concentration polarization, and as the interfacial Li^+ concentration approaches zero, a space-charge region forms near the electrode surface. The resulting steep electric-field gradients focus ionic flux toward surface protrusions, accelerating dendrite elongation and intensifying morphological inhomogeneity.

2.2 | Relationship Between Lithiophilic Components and Li Dendrite Growth

Lithiophilic components—defined as materials, phases, or surface functionalities with a strong thermodynamic affinity for Li—play a crucial role in dictating the nucleation dynamics and the resulting morphology of Li deposits in LMAs [35–38]. The strength of the interaction between Li atoms and the host surface can be quantitatively characterized by parameters such as binding energy, interfacial energy, and wetting angle (Figure 1d) [39]. Surfaces with high lithiophilicity possess lower Li–surface interfacial energies, thereby markedly reducing the nucleation overpotential. As a result, Li^+ ions preferentially deposit at numerous energetically favorable sites, producing a dense array of uniformly distributed nuclei. Such homogeneous nucleation suppresses localized current concentration and mitigates the formation of anisotropic protrusions that would otherwise evolve into dendrites.

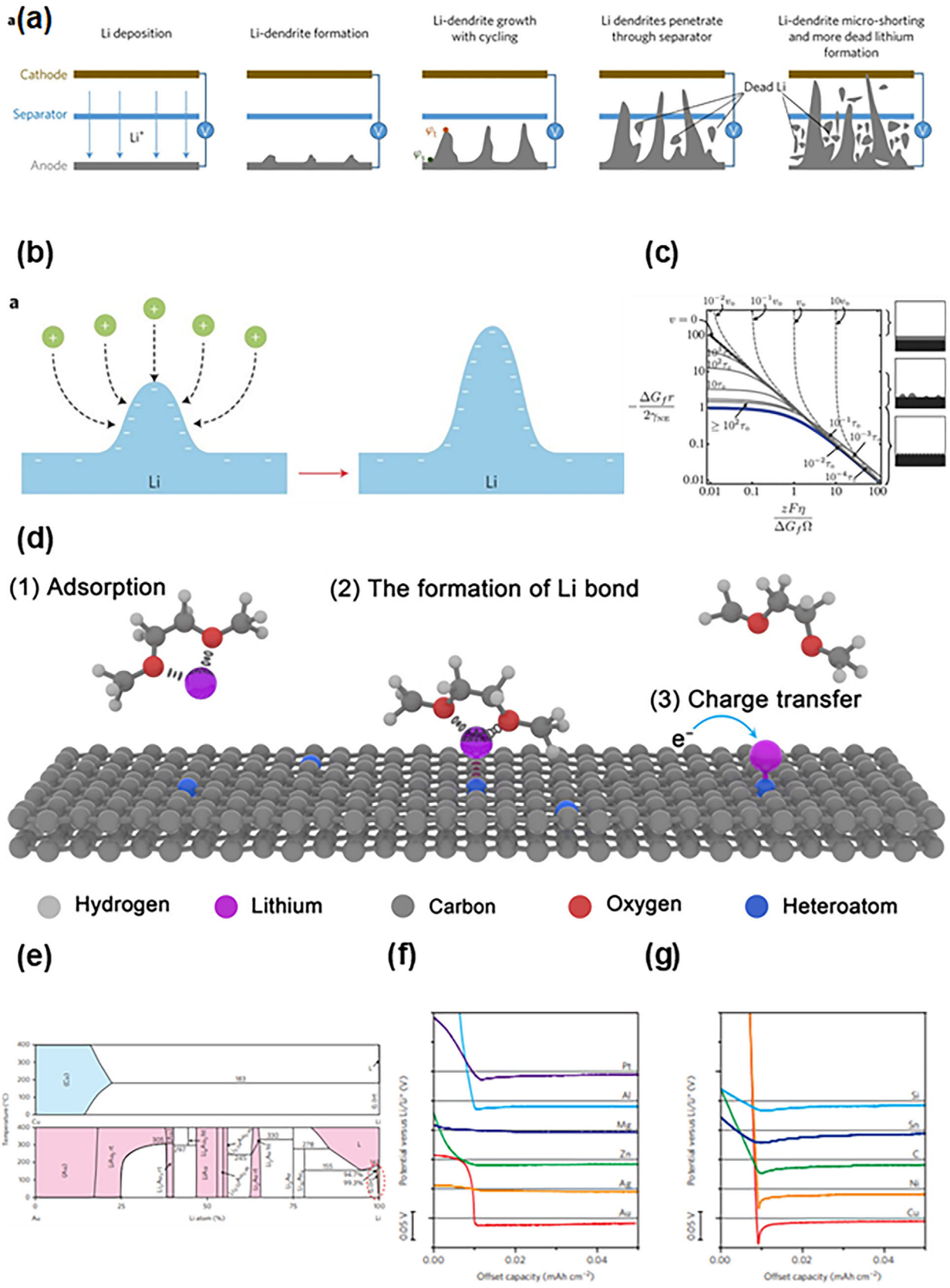

FIGURE 1 | (a) Schematic illustration of the cell failure mechanism induced by Li dendrite growth. Reproduced with permission.[26] Copyright 2017, Springer Nature. (b) Schematic illustration of the Li dendrite growth mechanism during Li deposition. Reproduced with permission.[31] Copyright 2017, Springer Nature. (c) A map of behavioral regimes for electrodeposition, plotting nucleus size against overpotential. The diagram distinguishes a nucleation suppression regime (below blue curve) and a stable growth regime (above black curve), with a long incubation time regime in between. Solid and dotted gray curves correspond to the loci of constant incubation times and initial growth velocities, respectively. Reproduced with permission.[32]

In contrast, lithiophobic or chemically heterogeneous surfaces exhibit higher interfacial energies and a scarcity of favorable adsorption sites, leading to sparse nucleation. Under these conditions, Li^+ ions are funneled toward a limited number of active sites, sharply increasing the local current density. This localized current focusing accelerates the vertical growth of Li deposits, resulting in needle-like or dendritic structures [40]. Upon repeated plating/stripping cycles, these protrusions become increasingly pronounced as the current continues to concentrate at their tips due to electric-field intensification.

The advantages of lithiophilic components are particularly evident when these materials can form alloys with Li during cycling. For example, metals such as Ag, Au, Zn, and In form Li–metal alloys (e.g., Li—Ag, Li—Zn, Li—In) that exhibit low nucleation overpotentials and high Li diffusivities. Among them, Ag NPs stand out due to their cost-effectiveness, excellent electrical conductivity (~1.586×10^{-8} Ω m at 25°C), wide Li—Ag alloying range, and favorable alloying/dealloying potential (0–0.25 V vs. Li/Li^+) [41, 42]. These properties make Ag NPs ideal additives for stabilizing LMAs by facilitating uniform Li nucleation and effectively suppressing dendritic growth. Yan et al. further constructed phase diagrams distinguishing the dissolving and non-dissolving materials in Li (Figure 1e) [43]. Materials such as Au, Ag, Zn, Mg, Pt, and Al exhibit substantial solubility in Li, whereas C, Si, and Sn display negligible solubility in Li, with Cu and Ni notably unable to form Li alloys. When the nucleation overpotential was evaluated, the fully lithiated Au, Ag, Zn, and Mg exhibited zero overpotential during Li deposition (Figure 1f). For high-solubility metals such as Ag and Mg, the slope of the potential profile becomes flatter prior to the onset of Li deposition, consistent with the behavior of a single-phase metal dissolved in Li. Conversely, Al and Pt, which have relatively low solubility in Li, show small but measurable nucleation overpotentials of approximately 5 and 8 mV, respectively. Beyond reducing nucleation barriers, the Li-alloying process with lithiophilic components also promotes homogeneous Li^+ transport across the interface and forms mechanically robust interphases capable of accommodating the large volume fluctuations associated with Li plating and stripping. Similarly, polar functional groups such as —COOH, —OH, and —NH_2—introduced through organic linkers or polymer coatings—can form strong dipole–Li interactions or coordination bonds, thereby anchoring Li^+ ions and guiding their uniform deposition.

On the other hand, materials with no solubility in Li metal—such as Cu, Ni, C, Sn, and Si—were also investigated. As shown in Figure 1g, all five materials display distinct overpotentials for Li nucleation. Similar to Cu, Ni does not form any alloy compound phase with Li, exhibiting a nucleation overpotential of ~30 mV. In contrast, C, Sn, and Si can form alloy phases with Li; for instance, Si forms a Li-rich alloy ($Li_{15}Si_4$) at room temperature. However, because the crystal structure of $Li_{15}Si_4$ differs significantly from that of metallic Li, a residual nucleation overpotential (~13 mV) persists. Comparable behavior is observed for Sn and C, with corresponding overpotentials of ~16 and ~14 mV, respectively. For all materials lacking true solubility in Li metal, the variation in overpotential values likely reflects differences in their intrinsic thermodynamic interactions with Li.

In 3D porous host architectures, the strategic distribution of lithiophilic components throughout the internal surface area further amplifies these advantages [44, 45]. The enlarged surface area effectively reduces the local current density, while the uniformly dispersed lithiophilic sites promote isotropic Li growth within the porous framework, thereby suppressing uncontrolled filamentary propagation toward the separator. The detailed mechanisms and electrochemical implications of such 3D lithiophilic host designs will be discussed in a subsequent section.

2.3 | Influence of SEI Formation and Composition on Li Dendrite Growth

The SEI, which spontaneously forms when metallic Li comes into contact with the electrolyte, plays a central role in regulating Li deposition behavior and, consequently, dendrite formation (Figure 2a) [46, 47]. Acting as both an ionic conductor and an electronic insulator, the SEI allows Li^+ transport to the electrode surface while preventing continuous electrolyte decomposition. Its physicochemical characteristics—composition, thickness, ionic conductivity, mechanical robustness, and uniformity—critically determine the nucleation growth and morphology of Li deposits.

A uniform, chemically homogeneous SEI with high ionic conductivity and sufficient mechanical strength enables uniform Li^+ flux across the electrode surface, thereby lowering local current density and promoting dense, isotropic Li deposition [48–52]. Inorganic-rich SEIs, composed primarily of LiF, Li_2O, Li_2CO_3, and Li_3N, typically exhibit high mechanical modulus, superior fracture toughness, and low electronic conductivity [53]. These properties stabilize the electrode/electrolyte interface and effectively suppress dendrite initiation (Figure 2b) [54]. For example, LiF-rich SEIs derived from fluorinated electrolytes possess high interfacial energy and elastic modulus, allowing them to resist deformation and tip growth under plating conditions (Figure 2c) [55].

In contrast, organic-rich SEIs—commonly formed via the decomposition of carbonate-based electrolytes—tend to be mechanically weaker, chemically less stable, and more heterogeneous in ionic conductivity at room temperature (Figure 2d) [56–58]. Such fragile interphases are prone to cracking and localized thinning during the substantial volume changes that accompany Li plating and stripping. These defects act as preferential Li^+ transport

Copyright 2013, The Electrochemical Society. (d) Schematic illustration of the Li nucleation mechanism on conductive scaffolds. Reproduced with permission.[39] Copyright 2019, American Association for the Advancement of Science (AAAS). (e) Binary phase diagrams for the Li—Cu (top) and Li—Au (bottom) systems. In the diagrams, "L" denotes the liquid phase, and "(Li)rt" represents the solid Li phase at room temperature. Reproduced with permission.[43] Copyright 2016, Springer Nature. Voltage profiles for materials (f) with some solubility in Li and (g) with negligible solubility in Li. Reproduced with permission.[43] Copyright 2016, Springer Nature.

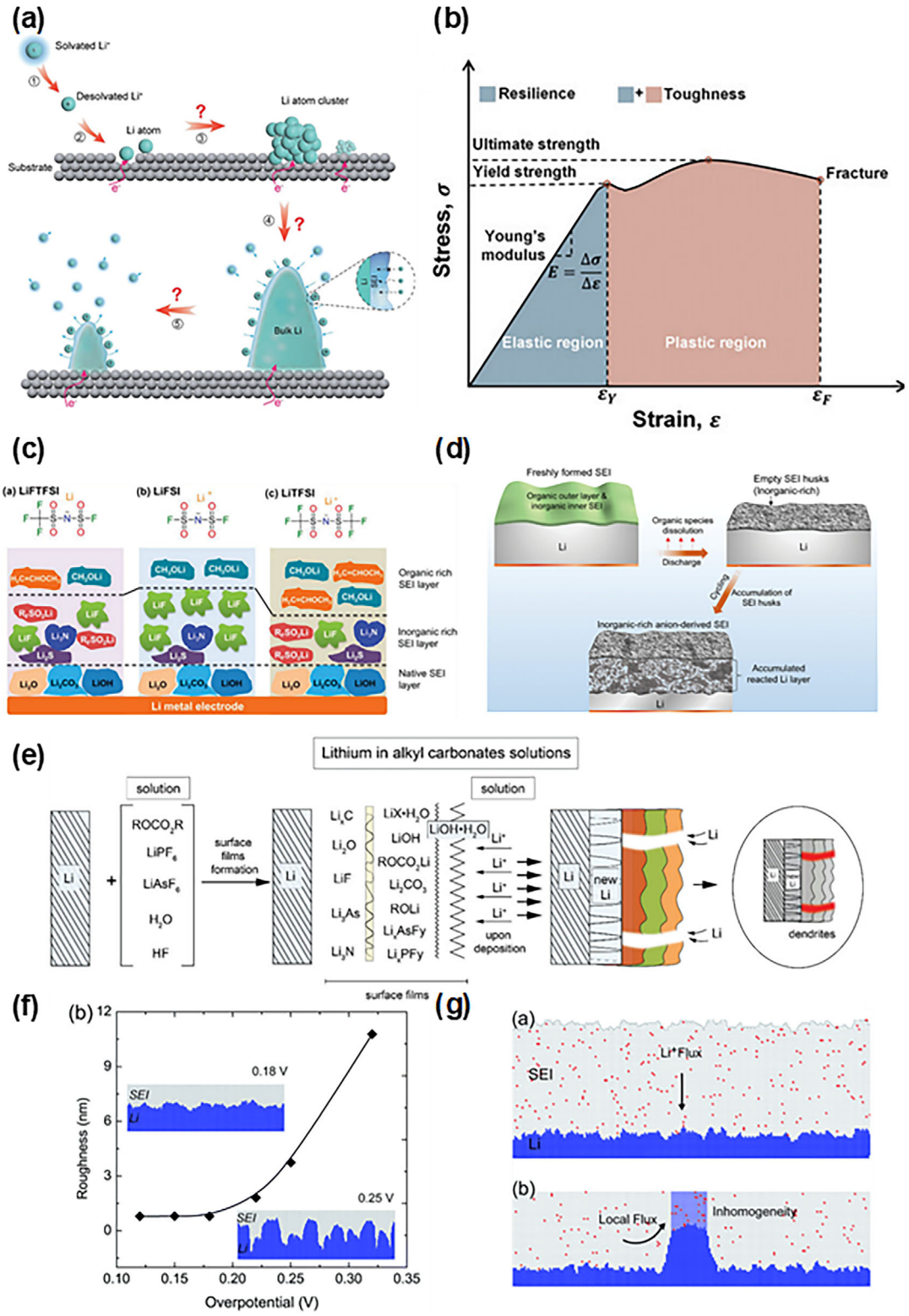

FIGURE 2 | (a) Schematic illustration of the mechanism of Li plating and stripping. Reproduced with permission.[46] Copyright 2022, Wiley-VCH. (b) Fundamental mechanical properties of the SEI layer illustrated by a typical stress-strain curve for an elastic-plastic material. Reproduced with permission.[54] Copyright 2022, Wiley-VCH. (c) Schematic illustration of the SEI layer formed on the surface of a Li metal electrode. Reproduced with permission.[55] Copyright 2021, Wiley-VCH. (d) Schematic illustration of the formation mechanism of an inorganic-rich, anion-derived SEI. Reproduced with permission.[56] Copyright 2024, Wiley-VCH. (e) Schematic illustration of the SEI formation on a Li metal electrode in an alkyl carbonate-based electrolyte. Reproduced with permission.[59] Copyright 2023, Wiley-VCH. (f) The effect of local overpotential on the nanoscale roughness of the Li metal–SEI interface, simulated at 300 K. The insets present two representative interface morphologies. Reproduced with permission.[60] Copyright 2018, Royal Society of Chemistry (RSC). (g) Simulation of the mechanism of Li deposition on a Li metal electrode with an inhomogeneous SEI. Red and blue circles represent Li ions and deposited Li atoms, respectively. Reproduced with permission.[60] Copyright 2018, Royal Society of Chemistry (RSC).

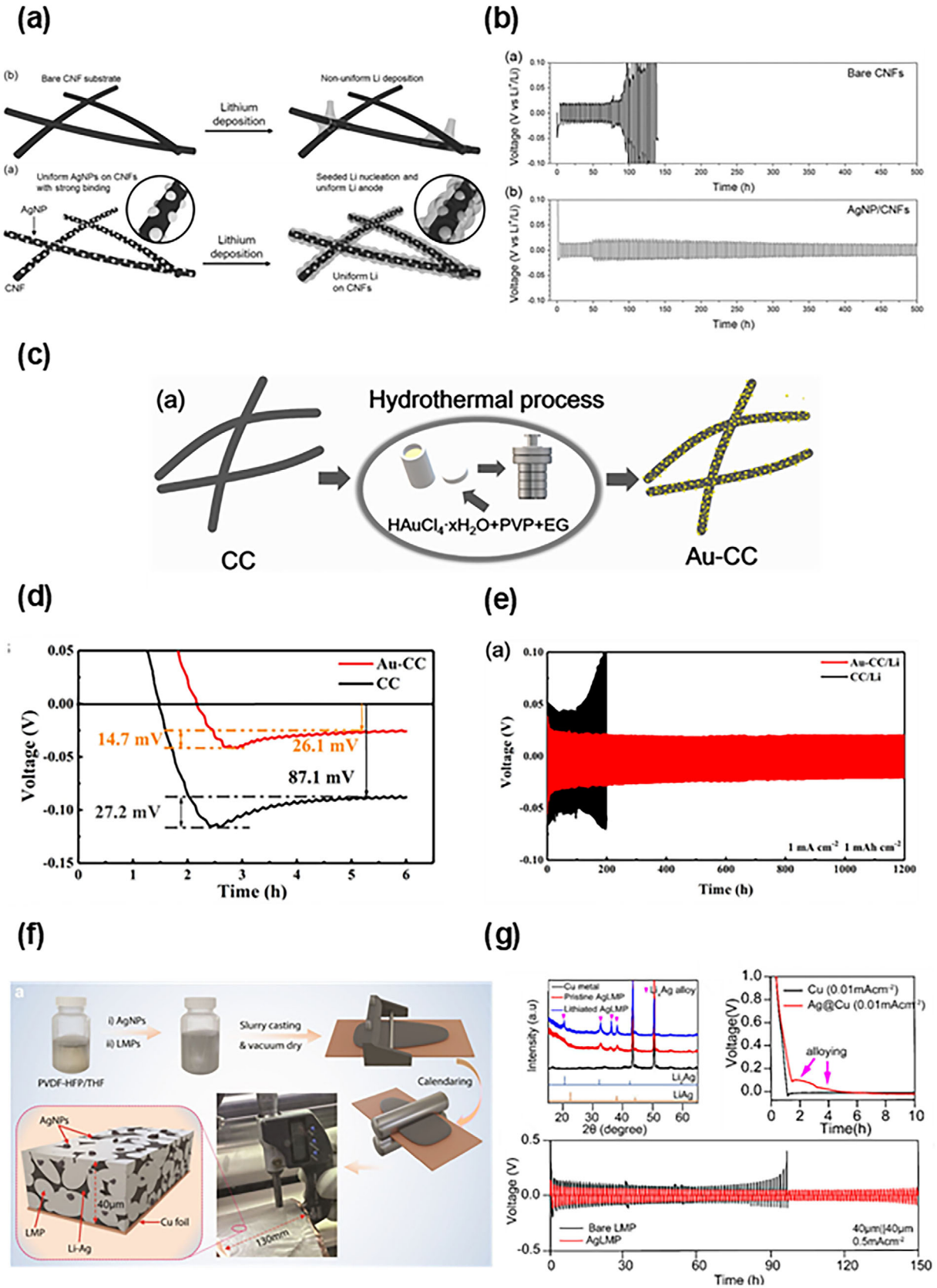

FIGURE 3 | (a) Schematic illustration of the Li deposition behavior on bare carbon nanofiber (CNF) and Ag NP-coated CNF. Reproduced with permission.[71] Copyright 2017, Wiley-VCH. (b) Cycling performance of symmetric cells with bare CNF and Ag NP-coated CNF at 0.5 mA cm^{-2} and 1 mAh cm^{-2}. Reproduced with permission.[71] Copyright 2017, Wiley-VCH. (c) Schematic illustration of the synthesis of Au-CC by hydrothermal process. Reproduced with permission.[72] Copyright 2021, Elsevier. (d) Voltage profiles of half cells with bare CC and Au-CC during the initial Li plating at 1 mA cm^{-2}. Reproduced with permission.[72] Copyright 2021, Elsevier. (e) Cycling performance of symmetric cells with bare CC and Au-CC at 1 mA cm^{-2} and

channels, concentrating current at protrusions and accelerating dendritic growth. Furthermore, SEIs containing electronically conductive impurities or decomposed byproducts can promote subsurface Li deposition, leading to filament growth beneath the interphase (Figure 2e) [59].

The dynamic evolution of the SEI during repeated cycling further exacerbates dendrite formation (Figure 2f,g) [60]. Continuous SEI fracture and reformation consume both electrolyte and active Li, elevate interfacial resistance, and generate spatially nonuniform surface energy landscapes. Such instability promoted tip-directed deposition in subsequent cycles, particularly under high current densities or ion transport-limited conditions. Therefore, durable dendrite suppression necessitates not only the initial optimization of SEI chemistry—through tailored electrolytes, additives, or artificial interfacial coatings—but also the long-term preservation of its structural and chemical integrity throughout cycling.

3 | Lithiophilic and Structural Modification of Host Electrodes

At the molecular level, host-electrode engineering is designed to reduce the Li nucleation barrier through the introduction of high-affinity binding sites (e.g., polar/charged functional groups and alloying or coordination centers), while simultaneously preserving continuous electronic transport pathways. Because these sites mediate Li^+ adsorption and desolvation, their interaction strength and spatial density dictate interfacial kinetics and ultimately determine nucleation uniformity. Accordingly, incorporating lithiophilic components into host electrodes effectively reduces the nucleation overpotential by providing energetically favorable sites that guide uniform Li nucleation across the electrode surface, thereby mitigating localized current concentrations and suppressing the formation of anisotropic protrusions that can evolve into dendrites. When integrated into 3D host architectures, these modifications further homogenize Li^+ flux throughout the electrode and accommodate the substantial volume fluctuations during repeated cycling, enabling dense and isotropic Li deposition with improved cycling stability and safety in LMBs. In the following section, we discuss representative lithiophilic and structural host-engineering strategies and their synergistic contributions to dendrite suppression.

3.1 | Lithiophilic-modified Host Electrodes

A widely adopted strategy for mitigating dendrite formation involves modifying host electrode surfaces with lithiophilic components that serve as energetically favorable nucleation sites for Li deposition. By introducing abundant and uniformly distributed Li-affinitive sites, such surface modifications promote spatially homogeneous Li nucleation, effectively alleviating localized current density spikes and suppressing anisotropic dendrite growth [61–64].

Early studies revealed that alloy-forming metallic coatings—such as Ag, Au, and Zn—can substantially lower the Li nucleation barrier [65–68]. Yang and co-workers demonstrated that Ag nanoparticle (NP)-coated 3D carbon hosts enable homogeneous Li nucleation through Li—Ag alloy formation, thereby achieving dendrite-free deposition over prolonged cycling (Figure 3a,b) [69–71]. Similarly, Chen et al. reported an Au-modified carbon cloth (Au-CC) framework, prepared by the chemical reduction of Au ions onto the carbon cloth surface, as an effective dendrite-free host for LMAs (Figure 3c). The strong Li—Au alloying interaction provided highly lithiophilic nucleation sites, guiding uniform and isotropic Li deposition throughout the 3D conductive network. Consequently, the Au-CC anode with low nucleation overpotential (14.7 mV) exhibited excellent cycling stability (Figure 3d), sustaining symmetric cell operation for over 1200 h at 1 mA cm^{-2} and 1 mAh cm^{-2}, with consistently high Coulombic efficiency during extended cycling (Figure 3e) [72]. More recently, Ssendagire et al. reported the fabrication of Ag nanoparticle–incorporated Li metal powder (AgLMP), enabling the production of Li metal anodes that are both wider and thinner than conventional Li foils (Figure 3f). The resulting 40 μm-thick AgLMP anode demonstrated the outstanding cycling stability, maintaining symmetric cell operation for more than 1200 h at 0.5 mA cm^{-2} and 0.5 mAh cm^{-2} (Figure 3g) [73].

However, in the case of Ag-based materials with strong lithiophilicity, their thermodynamic instability and kinetic limitations during electrochemical cycling can hinder the sustained formation of an effective lithiophilic surface. Specifically, the low cohesive energy of metallic silver makes Ag atoms highly prone to surface diffusion and Ostwald ripening, resulting in spontaneous metallic fusion (sintering) even at ambient temperature when interparticle separations are less than ~5 Å [74–77]. This phenomenon destabilizes the lithiophilic surface and decreases the effective density of active lithiophilic sites.

To address these limitations, various inorganic oxides have been explored as stable lithiophilic hosts [78–81]. For example, Chen et al. reported that laser-induced silicon oxide-coated Cu foils, derived from commercial adhesive tapes, form the stable Li–SiO_x alloys during plating. This alloying behavior lowers the nucleation barrier and enables smooth Li deposition profiles even under high current densities, resulting in excellent cycling stability for over 250 cycles with an average Coulombic efficiency of 99.3% at 2 mA cm^{-2} and 2 mAh cm^{-2}) (Figure 4a,b) [82]. Yan et al. constructed indium tin oxide (ITO) arrays on Cu current collectors using the magnetron sputtering method. Upon lithiation, the ITO arrays transformed into Li—In, Li—Sn, and Li_2O phases, which reduced Li diffusion barriers and promoted dense, uniform Li growth (Figure 4c) [83]. Owing to excellent

1 mAh cm^{-2}. Reproduced with permission.[72] Copyright 2021, Elsevier. (f) Schematic illustration and digital image of the preparation of AgLMP anode. Reproduced with permission.[73] Copyright 2021, American Chemical Society. (g) XRD patterns of AgLMP anode before and after lithiation, which are drawn along with the simulated XRD patterns of LiAg and Li_2Ag intermetallic compound (top left). Voltage profiles of half cells with bare LMP and AgLMP during the initial Li plating at 0.01 mA cm^{-2} (top right). Cycling performance of 40μm thick Li//40μm thick Li symmetric cells with bare LMP and AgLMP at 0.5 mA cm^{-2} and 0.125 mAh cm^{-2} (bottom). Reproduced with permission.[73] Copyright 2021, American Chemical Society.

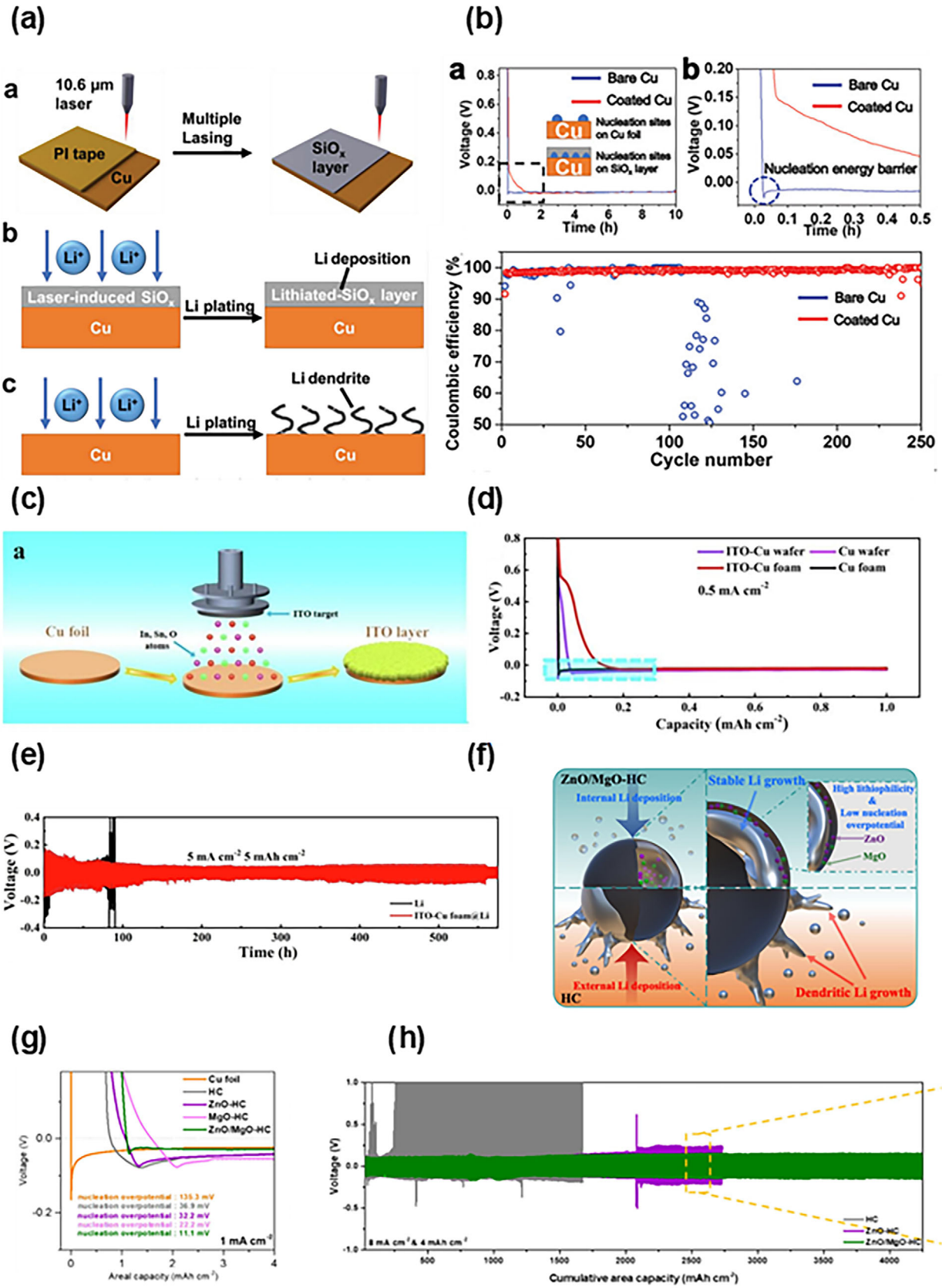

FIGURE 4 | (a) Schematic illustration of Li-SiO_x layer on the Cu current collector by multiple lasings and Li deposition on bare Cu foil and Laser-induced (LI) – SiOx coated Cu foil. Reproduced with permission.[82] Copyright 2020, Wiley-VCH. (b) Voltage profiles of half cells with bare Cu foil and LI-SiOx coated Cu foil during the initial Li plating at 0.1 mA cm^{-2} (top). Coulombic efficiency of half cells with bare Cu foil and LI-SiOx coated Cu foil at 0.5 mA cm^{-2} and 0.125 mAh cm^{-2} (bottom). Reproduced with permission.[82] Copyright 2020, Wiley-VCH. (c) Schematic illustration of preparing ITO-Cu wafer electrode via magnetic sputtering method. Reproduced with permission.[83] Copyright 2022, Elsevier. (d) Voltage profiles of half cells

wettability and even self-propagation behavior between ITO-Cu and molten Li, the half cells with ITO-Cu electrodes exhibit an ultralow nucleation overpotential of 2 mV at 0.5 mA cm^{-2} (Figure 4d). Additionally, the ITO-Cu@Li symmetric cell also demonstrated remarkable cycling stability for over 1000 h at a current density of 1 mA cm^{-2} and a capacity of 1 mA cm^{-2} (Figure 4e).

Recently, Park et al. proposed hollow carbon (HC) structures incorporating ZnO and MgO nanoparticles as advanced lithiophilic frameworks for LMAs (Figure 4f) [84]. In this design, ZnO provides strong lithiophilicity, selectively interacting with Li^+ ions, while MgO effectively lowers the nucleation overpotential. Encapsulating both oxide components within the hollow carbon shell confines Li deposition to the internal cavity, thereby promoting uniform and stable Li growth and forming a mechanically robust and durable anode. Under half-cell conditions, the ZnO/MgO-HC electrode exhibited a remarkably low nucleation overpotential (11.1 mV) and a low charge transfer resistance (R_{ct}) of 17.20 Ω. Furthermore, the symmetric cell with the ZnO/MgO-HC electrode demonstrated excellent cycling stability for over 1500 h at a current density of 1 mA cm^{-2} and a capacity of 1 mAh cm^{-2} (Figure 4g,h).

However, despite these advances, in most cases, depositing lithiophilic metals or oxides onto host electrodes using conventional slurry coating—without incorporating complementary interfacial interactions—leads to the formation of relatively thick layers (typically several to tens of micrometers) containing polymeric binders. Such binder-rich coatings not only decrease the specific energy density of LMAs but also restrict their applicability to host electrodes with complex geometries or irregular surfaces.

3.2 | 3D-structured Host Electrodes

Host materials with a 3D architecture and high electronic conductivity have emerged as promising platforms for mitigating dendrite growth in LMAs. Such structures can effectively reduce local current density, provide a large-area lithiophilic surface that promotes uniform Li nucleation, and accommodate volume changes during repeated cycling. To date, a wide range of 3D host materials has been developed, which can generally be classified into metal-based analogues (e.g., Cu foam, Ni foam) [85, 86] and carbon-based counterparts (e.g., CNTs, graphene, reduced graphene oxide (rGO), carbon cloth, porous carbon) [87–89].

Metal-based 3D scaffolds, while highly conductive, are often limited by their high mass density and large volume, which reduce both volumetric and gravimetric energy densities. Moreover, their limited flexibility and mechanical brittleness hinder practical application in flexible or compact battery designs. In contrast, carbon-based substrates overcome many of these drawbacks, offering advantages such as wide availability, low cost, high thermal stability, mechanical flexibility, and low mass density. Nevertheless, with the exception of rGO, most carbon-based materials are intrinsically lithiophobic and thus require surface modification to introduce lithiophilic characteristics. In the case of carbon cloth or carbon fiber cloth (shortly CFC), the surface modification strategies commonly include heteroatom element doping (i.e., O doping, N/S/P co-doping) [39, 90, 91], defect engineering [92–94], or polar functional group grafting (—COOH, —C═O, —OH, —NH, and —NH_2) [95–97]. Each approach effectively tailors the surface electron distribution, enhances Li affinity, and promotes uniform deposition.

As a representative example of polar functional group grafting, Wang et al. reported a nanostructured carbon fiber cloth (CFC)@Li composite prepared by electro-deposition process, where the CFC substrate was pre-activated using nitric acid to introduce oxygen-containing groups (e.g., —OH, —COOH) onto the carbon fiber surface (Figure 5a) [98]. These oxygenated sites served as strong electrostatic anchors for Li nucleation, enabling the CFC@Li anode to exhibit a low overpotential of 18 mV and an extended cycling lifespan exceeding 350 h at a high current density of 4.0 mA cm^{-2} and a large areal capacity of 10.0 mAh cm^{-2} (Figure 5b). Likewise, Niu et al. developed amine (NH_2)-functionalized mesoporous CNFs, where the NH_2 groups significantly improved lithiophilicity, and the mesoporous surface acted as preferential Li^+ nucleation sites, leading to self-smoothing Li deposition and effective dendrite suppression (Figure 5c) [99]. Full cells pairing this composite LMA with commercial NMC622 or NMC811 ($LiNi_{0.8}Mn_{0.1}Co_{0.1}O_2$) cathodes delivered high energy densities of 350–380 Wh kg^{-1} and stable cycling for up to 200 cycles (Figure 5d).

Unlike carbon cloth or carbon fiber cloth, which offer high electrical conductivity but limited surface area, insulating textile substrates provide much larger surface area due to their fibrillar network structure. To function as current collectors, however, these insulating textiles must be rendered electrically conductive. In most cases, conductive textiles have been fabricated by i) depositing solution-processable conductive components—such as carbon nanotubes (CNTs) [100–102] or conducting polymers [103, 104]—or (ii) employing electroless plating (i.e., chemical reduction) methods [105, 106] to deposit metallic layers from metal ion precursors. Recently, Cai et al. demonstrated the rapid fabrication of thin, stable LMAs through selective wetting of molten Li onto one side of a conductive textile prepared by chemical reduction of Ni ions, achieving a uniform Li coating (~3.0 mg cm^{-2}) on one face of the framework (Figure 5e) [107].

with bare Cu wafer, ITO-Cu wafer, bare Cu foam, ITO-Cu foam during the initial Li plating at 0.5 mA cm^{-2}. Reproduced with permission.[83] Copyright 2022, Elsevier. (e) Cycling performance of symmetric cells with bare Li and Li plated ITO-Cu foam at 1 mA cm^{-2} and 1 mAh cm^{-2}. Reproduced with permission.[83] Copyright 2022, Elsevier. (f) Schematic illustration of the Li plating and stripping process on bare HC and ZnO/MgO-HC. Reproduced with permission.[84] Copyright 2024, Elsevier. (g) Voltage profiles of half cells with bare Cu foil, bare HC, ZnO-HC, MgO-HC and ZnO/MgO-HC during the initial Li plating at 1 mA cm^{-2}. Reproduced with permission.[84] Copyright 2024, Elsevier. (h) Cycling performance of symmetric cells with bare HC, ZnO-HC and ZnO/MgO-HC at 1 mA cm^{-2} and 1 mAh cm^{-2}. Reproduced with permission.[84] Copyright 2024, Elsevier.

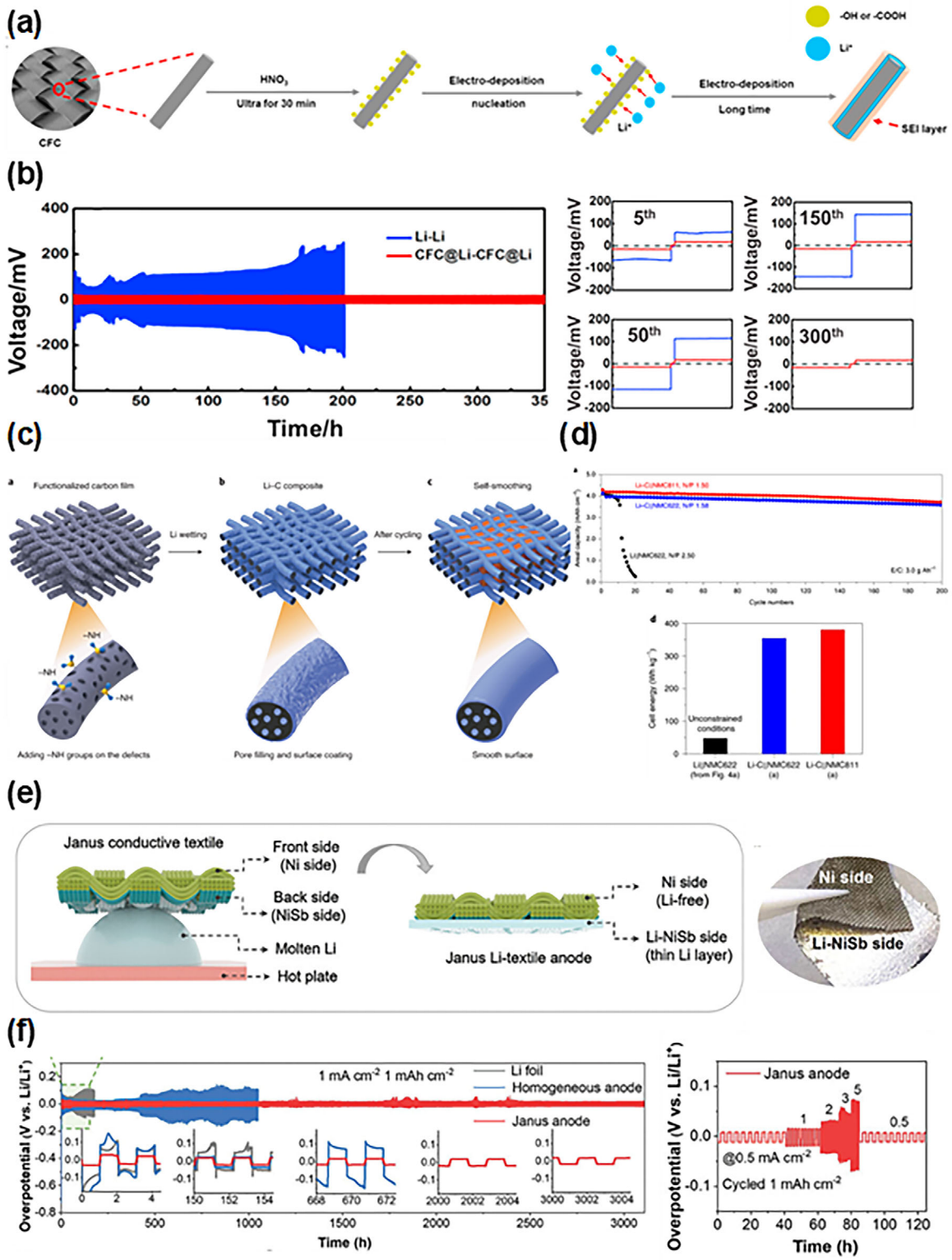

FIGURE 5 | (a) Schematic illustration of fabrication process of CFC with stable SEI layers by the electro-deposition method. Reproduced with permission.[98] Copyright 2018, Elsevier. (b) Cycling performance of symmetric cells with bare Li foil and Li plated CFC (left) and detailed voltage profiles at different cycles (right) at 4 mA cm^{-2} and 10 mAh cm^{-2}. Reproduced with permission.[98] Copyright 2018, Elsevier. (c) Schematic illustration of the fabrication process and self-smoothing behavior of a Li—C anode. Reproduced with permission.[99] Copyright 2019, Springer Nature. (d) Cycling performance of asymmetric full cells with Li—C||NMC811, Li—C||NMC622 and Li||NMC622 cells at a C/5 charge and a C/3 discharge (top) and estimated energy densities (bottom). Reproduced with permission.[99] Copyright 2019, Springer Nature. (e) Schematic illustration of the selective-wetting mechanism of molten Li on the Janus Li-textile anode (left) and digital image of the Janus Li-textile anode (right). Reproduced with permission.[107] Copyright 2023, Wiley-VCH. (f) Cycling performance of symmetric cells with bare Li foil, homogeneous Li-textile anode and Janus Li-textile anode at 1 mA cm^{-2} and 1 mAh cm^{-2} (left) and rate capability of Janus Li-textile anode (right). Reproduced with permission.[107] Copyright 2023, Wiley-VCH.

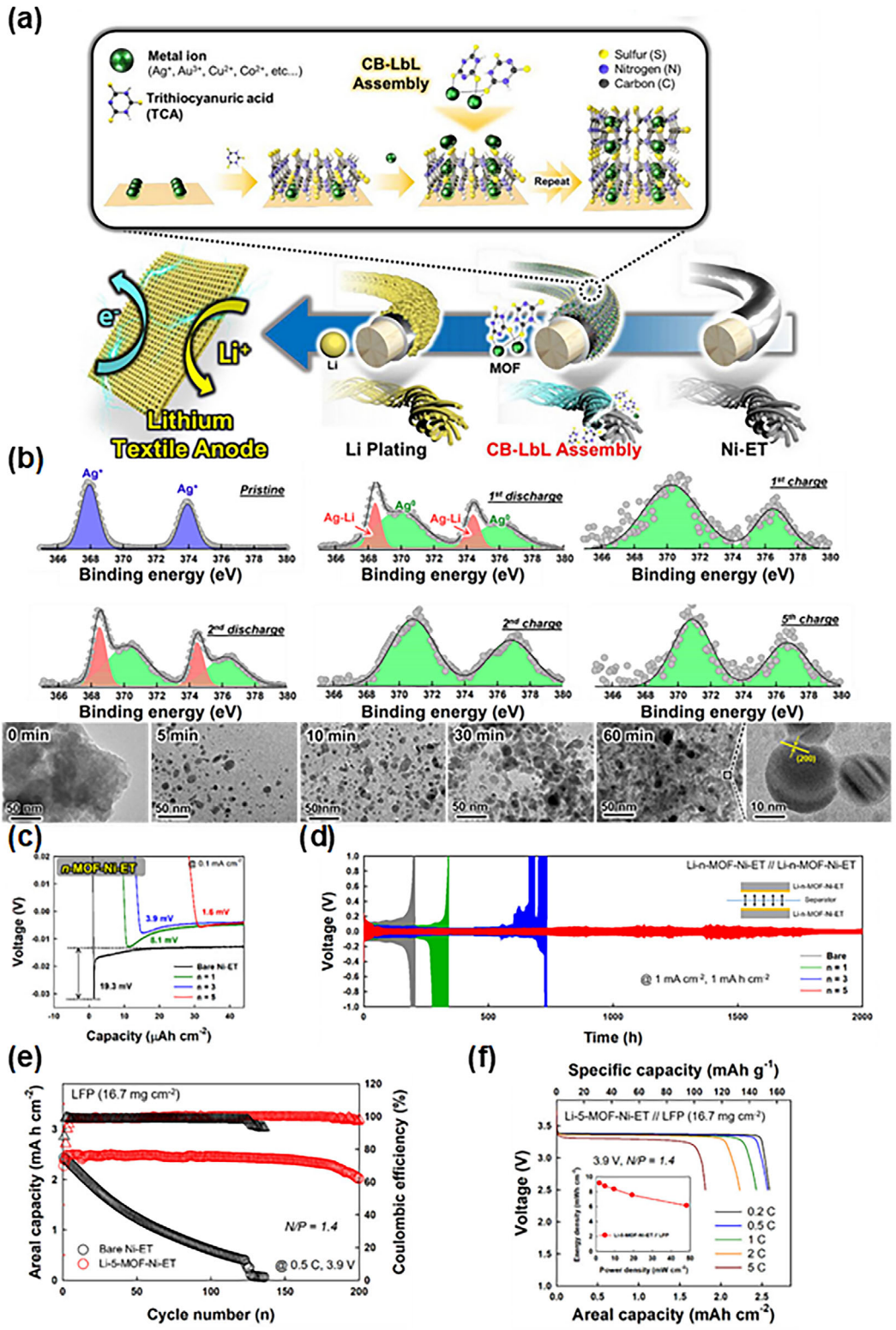

FIGURE 6 | (a) Schematic illustration for the preparation of Li textile anode using interfacial interaction-mediated ultrathin MOF multilayers. Reproduced with permission.[108] Copyright 2025, Wiley-VCH. (b) Ag 3d XPS spectra of 5-MOF-Ni-ET during the Li plating/stripping cycles (top) and HR-TEM images of $[Ag^+/TCA]_5$-MOF multilayers during the initial Li plating at 0.1 mA cm^{-2} for 0 (bare), 5, 10, 30, and 60 min (bottom). Reproduced with permission.[108] Copyright 2025, Wiley-VCH. (c) Voltage profiles half cells with bare Ni-ET and n-MOF-Ni-ET during the first Li plating at 0.1 mA cm^{-2}. Reproduced with permission.[108] Copyright 2025, Wiley-VCH. (d) Cycling performance of symmetric cells with bare Ni-ET and n-MOF-Ni-ET at 1 mA cm^{-2},1 mAh cm^{-2}. Reproduced with permission.[108] Copyright 2025, Wiley-VCH. (e) Cycling performance of asymmetric full cells with bare Ni-ET//LFP and 5-MOF-Ni-ET//LFP at cathode mass loading of 16.7 mg cm^{-2}. Reproduced with permission.[108] Copyright 2025, Wiley-VCH. (f) Current density-dependent discharge profiles of asymmetric full cells with Ni-ET//LFP at cathode mass loading of 16.7 mg cm^{-2}. The inset presents the energy and power densities at varying current densities. Reproduced with permission.[108] Copyright 2025, Wiley-VCH.

This Janus Li–textile composite anode reduced Li consumption by approximately 80% compared to homogeneous composites and enhanced cycling stability through the synergistic effects of a lithiophobic–lithiophilic framework design and an upper buffering space. At a high depth of discharge (75%), the Janus Li–textile anode maintained an ultralong cycle life exceeding 3000 h (Figure 5f).

Nevertheless, current approaches still face challenges in precisely controlling interfacial interactions between insulating textile substrates and conductive coatings—particularly in chemically reduced metal layers—as well as between adjacent conductive components. These limitations often result in suboptimal electrical conductivity, non-uniform coating coverage, and partial blockage of the intrinsic porosity of the textile network. Such drawbacks compromise the inherent advantages of textile-based hosts, which depend on high lithiophilic surface area and the ability to buffer mechanical deformation during cycling.

To overcome these limitations, Nam et al. recently developed a high-performance, dendrite-free Li textile anode that exhibited both high capacity and long-term cycling stability (Figure 6a) [108]. This achievement was realized by a repeated coordination bonding-based layer-by-layer (LbL) assembly of Ag^+ ions and trithiocyanuric acid (TCA), which generated uniform and ultrathin metal–organic framework (MOF) multilayers (<40 nm) on Ni-electroplated polyester textiles. During electrochemical operation, the Ag^+ ions within the MOF were in situ chemically reduced to form highly lithiophilic Ag NPs, significantly lowering the Li nucleation barrier (Figure 6b,c). The symmetric cells incorporating LbL-assembled $(Ag^+/TCA)_5$ MOF multilayers demonstrated the outstanding cycling stability for over 2000 h at 1 mA cm^{-2} and 1 mAh cm^{-2} (Figure 6d). Furthermore, full cells paired with an LFP cathode and a low N/P ratio of 1.4 retained 92% of their initial capacity over 180 cycles (Figure 6e). As a result, the ultrathin MOF multilayer–assembled anode achieved high areal energy and power densities of 9.14 mWh cm^{-2} and 48.3 mW cm^{-2}, respectively (Figure 6f). A quantitative comparison of representative electrode-modification strategies and their electrochemical performance is summarized (Table 1), while the corresponding systematic comparisons are summarized (Table 2).

Importantly, a fundamental challenge in anode-free LMB systems lies in achieving uniform and reversible Li nucleation and growth on the initial host substrate. In the absence of pre-existing lithiophilic sites, Li nucleation is governed by a high energetic barrier, which intrinsically favors spatially heterogeneous deposition. Such nonuniform nucleation behavior gives rise to localized current amplification, leading to irregular Li morphologies and accelerating the formation of electronically isolated "dead Li." Moreover, the Li metal interface in anode-free configurations is inherently thin and dynamically evolving; during repeated plating/stripping cycles, this fragile interface is particularly susceptible to pronounced geometric instabilities, including surface roughening, interfacial delamination, and loss of interfacial contact. These degradation pathways are further intensified under practically relevant operating conditions, such as high current densities and lean electrolyte environments, where kinetic and mechanical stresses are simultaneously amplified [109].

Addressing these electrochemical and mechanical challenges places exceptionally stringent demands on interfacial chemistry and architectural design in anode-free LMBs. First, the current collector and/or separator must be modified with ultrathin, conformal, and lithiophilic interlayers that effectively lower the Li nucleation barrier while homogenizing Li^+ flux from the very first plating cycle. Second, beyond nucleation control, these interlayers must actively regulate solvent and anion coordination at the interface to direct the formation of a mechanically robust yet ionically conductive SEI. Third, because anode-free systems operate without any excess Li reservoir, precise suppression of parasitic side reactions—including electrolyte consumption, interfacial decomposition, and unintended electronic conduction pathways—is critical to maintaining high Coulombic efficiency over extended cycling.

Taken together, these considerations highlight that the realization of high-performance anode-free LMBs is dictated not solely by the selection of bulk functional materials but more fundamentally by the capability to engineer interfacial interactions with molecular-level precision. Such interaction-driven interfacial design provides the necessary leverage to couple controlled Li electrochemistry with long-term mechanical and chemical stability under demanding operating conditions.

Given the distinct advantages of these textile current collectors and interfacial interaction–driven ultrathin film technologies, this strategy holds great promise for broad implementation across diverse energy storage applications in the future.

4 | Separator Modification

Separator engineering regulates Li dendrites by controlling the near-interface Li^+ flux and the local chemical environment at the separator/anode boundary. These molecular-level interactions—electrostatic attraction/repulsion, polarity-driven wetting, and Li^+ coordination—collectively dictate ion-transport selectivity, interfacial concentration gradients, and the likelihood of heterogeneous nucleation. Accordingly, separator strategies can be broadly classified into (i) physical shielding/structural barriers and (ii) chemical functionalization/interaction-driven interlayers, which act either by impeding dendrite propagation or by tuning electrolyte affinity and interfacial ion transport to homogenize Li^+ flux and stabilize interphase chemistry.

The separator serves as a porous, electronically insulating membrane that physically isolates the cathode and anode while allowing efficient Li^+ transport through the liquid electrolyte. A hydrophilic surface of separator generally enhances compatibility with conventional polar electrolytes (e.g., carbonate- or ether-based solvents), thereby enhancing electrolyte uptake and retention within the porous framework and ensuring continuous ionic pathways for efficient ion conduction [110–113]. However, even with favorable electrolyte wettability, the Li^+ flux at the anode surface often becomes spatially non-uniform due to local variations in current density, surface roughness, and electrode defects, all of which strongly affect heterogeneous nucleation and dendritic growth [33, 114–116]. Because the separator is in direct contact with the anode surface, its interfacial properties critically

TABLE 1 | Electrochemical performance comparison of the reported electrodes in LMA.

Material	Method	Thickness	Symmetric Cell Performance	Asymmetric Full Cell Performance	References
Ag NPs	Electric Joule heating	~40nm (NP size)	500 h @ 0.5 mA cm^{-2} / 1 mAh cm^{-2} 400 h @ 1 mA cm^{-2} / 2 mAh cm^{-2}	–	[71]
Au	Hydrothermal	~32.4μm	~1200 h @ 1 mA cm^{-2} / 1 mAh cm^{-2} ~350 h @ 3 mA cm^{-2} / 1 mAh cm^{-2}	LFP : 75.1% after 300 cycles @ 1C LFP : 80.8% after 200 cycles @ 3C	[72]
Ag NPs/Li metal powder	Slurry – Blade coating	10μm (Ag coating thickness)	~150 h @ 1 mA cm^{-2} / 1 mAh cm^{-2}	NCM433 : 73.6% after 500 cycles @ 0.3C Charging, 0.5C Discharging NCM433 :>90% after 200 cycles @ 1C	[73]
SiO_x	Multiple Lasing	~200nm	–	LFP : :52.8% after 100 cycles @ 0.9 mA cm^{-2}	[82]
ITO	Magnetron sputtering	~100nm	1000 h @ 1 mA cm^{-2} / 1 mAh cm^{-2}	LFP : 103% after 1000 cycles @ 5C	[83]
ZnO/MgO	Precipitation – Dehydration	5μm	1500 h @ 1 mA cm^{-2} / 1 mAh cm^{-2} 500 h @ 1 mA cm^{-2} / 1 mAh cm^{-2}	LFP : 90.7% after 500 cycles @ 5C	[84]
—OH, —COOH	Acid treatment	–	1000 h @ 0.5 mA cm^{-2} / 10 mAh cm^{-2} 500 h @ 2 mA cm^{-2} / 10 mAh cm^{-2} 350 h @ 4 mA cm^{-2} / 10 mAh cm^{-2}	LFP : ~100% after 300 cycles @ 1C	[98]
Li—C	C : Electrospun Li : molten Li	–	–	NCM622 : 91% after 200 cycles @ C/5 Charging, C/3 Discharging NCM811 : 86% after 200 cycles @ C/5 Charging, C/3 Discharging	[99]
Ni, NiSb	Ni : Polymer-assisted metal deposition method Sb : Thermal evaporation	Ni : – Sb : 100nm	>3000 h @ 1 mA cm^{-2} / 1 mAh cm^{-2}	LCO : 99.94% after 2000 cycles @ 1C	[107]
$[Ag^+/TCA]_5$-MOF	Layer-by-Layer assembly	~39nm	~2000 h @ 1 mA cm^{-2} / 1 mAh cm^{-2} 950 h @ 3 mA cm^{-2} / 3 mAh cm^{-2}	LFP : 96.5% after 1300 cycles @ 1C	[108]

TABLE 2 | Systematic comparison of the reported electrodes in LMA.

Material	Method	Action Mechnaism	Key Advantages	Limitations	References
Ag NPs	Electric Joule heating	Seeded Li nucleation	Low nucleation overpotential	Process-sensitive Ag aggregation/poor anchoring	[71]
Au	Hydrothermal	Li—Au alloying (solid-solution)	Dendrite suppression	Au cost Micro-scale particles	[72]
Ag NPs/Li metal powder	Slurry – Blade coating	Li—Ag alloy layer	Scalable large-area thin Li anode fabrication	Slurry-cast electrode uses polymer binder	[73]
SiO_x	Multiple Lasing	Accommodate volume expansion	Dendrite-free deposition	Initial Li consumption	[82]
ITO	Magnetron sputtering	Alloy-anchoring	Ultralow overpotential	Site degradation	[83]
ZnO/MgO	Precipitation – Dehydration	Multi-seed lithiophilicity Solid-solution alloying	Internal Li confinement	Intermetallic-compound fragility	[84]
—OH, —COOH	Acid treatment	Alloy anchoring	Uniform deposition	Phase conversion Volume change	[98]
Li—C	C : Electrospun Li : molten Li	Wetting–confinement self-smoothing	Works under practical metrics with stable cycle	Requires molten-Li handling/infusion	[99]
Ni, NiSb	Ni : Polymer-assisted metal deposition method Sb : Thermal evaporation	Janus-wettability– guided deposition	Li-saving	Requires high-temperature molten Li	[107]
$[Ag^+/TCA]_5$- MOF	Layer-by-Layer assembly	Lithiophilic nucleation seeding	Ultrathin binder-free coating	Time consuming	[108]

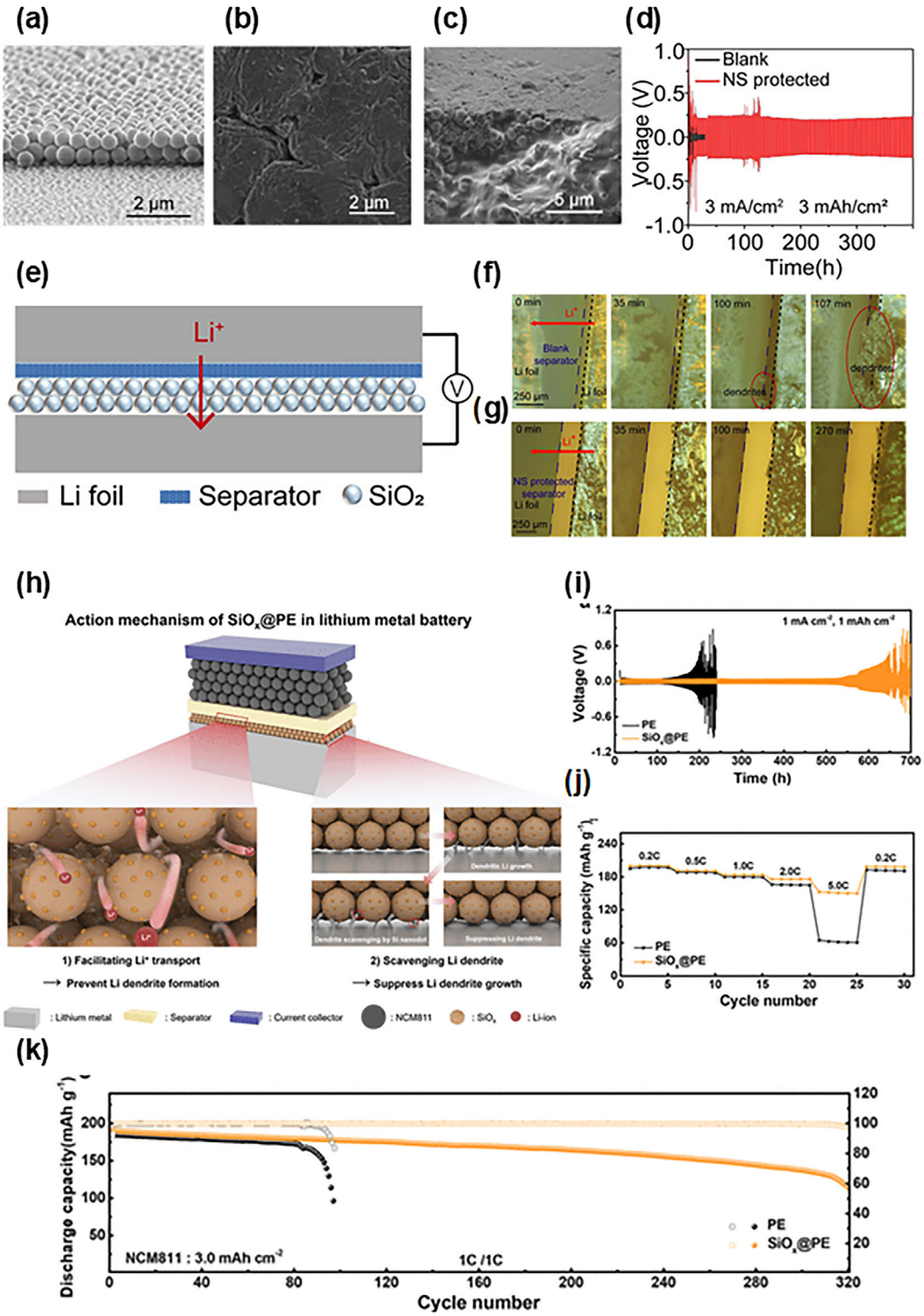

FIGURE 7 | (a) SEM image of the NS protected separator with SiO_2 spheres. Reproduced with permission.[127] Copyright 2020, Wiley-VCH. SEM images of Li foil after 200 cycles with nano-shield (NS) protected separators from (b) top view (c) cross-sectional view. Reproduced with permission.[127] Copyright 2020, Wiley-VCH. (d) Cycling performance of symmetric cells with blank separator and NS protected separator at 3 mA cm^{-2} and 3 mAh cm^{-2}. Reproduced with permission.[127] Copyright 2020, Wiley-VCH. (e) Schematic illustration of symmetric cells with NS protected separator. Reproduced with permission.[127] Copyright 2020, Wiley-VCH. Optical photographs of the discharged Li metal wrapped by separator during in-situ observation of Li dendrite growth process (f) with blank separator and (g) with NS protected separator. Reproduced with permission.[127] Copyright 2020, Wiley-VCH. (h) Schematic illustration of action mechanism of SiO_x@PE in LMB. Reproduced with permission.[130] Copyright 2025, American Chemical Society. (i) Cycling performance of symmetric cells with bare PE separator and SiO_x@PE separator at 1 mA cm^{-2} and 1 mAh cm^{-2}. Reproduced with permission.[130] Copyright 2025, American Chemical Society. (j) Rate capability at various C-rates and (k) cycling performance of asymmetric Li||NCM811 full cells with bare PE separator and SiO_x@PE separator at 1.0 C. Reproduced with permission.[130] Copyright 2025, American Chemical Society.

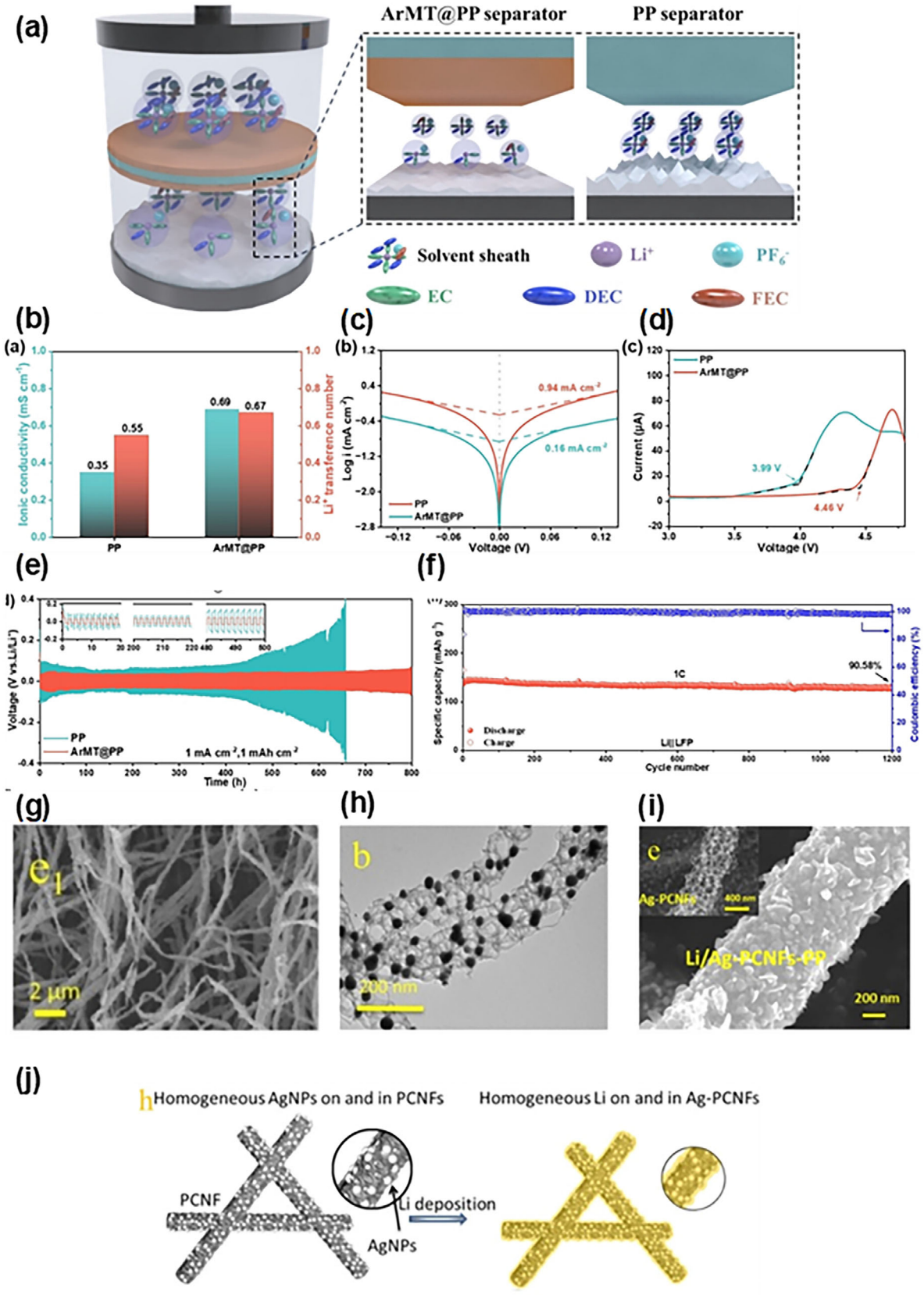

FIGURE 8 | (a) Schematic illustration of the Li ion solvation and transport behavior through the ArMT@PP separator compared with the bare PP separator. Reproduced with permission.[140] Copyright 2025, Wiley-VCH. (b) Ion conductivity and Li^+ transference number of the cells with PP and ArMT@PP separators. Reproduced with permission.[140] Copyright 2025, Wiley-VCH. (c) Tafel plot for Li plating/stripping of the symmetric cells with bare PP separator and ArMT@PP separator. Reproduced with permission.[140] Copyright 2025, Wiley-VCH. (d) LSV curve of Li||stainless steel half cells with bare PP separator and ArMT@PP separator. Reproduced with permission.[140] Copyright 2025, Wiley-VCH. (e) Cycling performance of

influence local ion-transport kinetics and the spatial distribution of Li^+ flux. Therefore, rational surface modification of the separator —via physical shielding or chemical functionalization—can effectively regulate Li^+ flux uniformity at the anode–separator interface, thereby reducing the local nucleation barriers, and suppress dendritic growth and penetration toward the cathode. In the following section, we discuss advanced separator surface engineering strategies, emphasizing their underlying mechanisms and potential to enhance the electrochemical performance of LMAs.

4.1 | Formation of Physical Barrier

Mechanical suppression of Li dendrite growth represents one of the most direct and straightforward approaches. Unlike approaches that primarily aim to prevent initial Li nucleation, this method focuses on physically blocking dendrites from penetrating the separator. Consequently, the mechanical properties of both the dendrite and the separator—particularly parameters such as elastic modulus, hardness, and fracture strength—become crucial determinants of performance. Typically, polycrystalline Li, which possesses a body-centered cubic (BCC) lattice structure, exhibits a Young's modulus of approximately 2–8 GPa and a yield strength in the range of 0.4–0.9 MPa [117], depending on factors such as grain size, defect density, and experimental conditions. Thermodynamically, Li dendrites preferentially grow along specific crystallographic orientations, most commonly the <111> or <110> directions of the BCC lattice, as their growth is kinetically governed by ion transport dynamics and surface energy minimization [118, 119]. This process favors the formation of oriented single-crystal structures with needle- or whisker-like morphologies, rather than the more reactive, randomly oriented polycrystalline aggregates. Moreover, size reduction in single crystalline structures leads to enhanced mechanical strength, as the absence of grain boundaries suppresses crack blunting, thereby increasing the likelihood of separator penetration and internal short circuits [120, 121].

To address these issues, the incorporation of inorganic solids—such as SiO_2, TiO_2, or Al_2O_3 NPs with sufficient mechanical robustness [122]—onto the separator surface has been widely explored to suppress Li dendrite propagation. In addition to their intrinsic strength, the surface oxygen atoms in these ceramic oxides possess strong electron-withdrawing properties, which improve electrolyte wettability and promote uniform Li^+ ion flux distribution [123–126]. For example, Liang et al. demonstrated that a spin-coated SiO_2 NP array on a commercial polyolefin separator effectively prevented dendrite penetration during repeated Li plating/stripping cycles, maintaining interfacial stability for 400 h at 3 mA cm^{-2} and 3 mAh cm^{-2} in a Li symmetric cells (Figure 7a–d) [127]. This improved performance was mainly attributed to stress redistribution: when the particle radius was comparable to the Li dendrite tip, nanosized spherical particles effectively dispersed local stress and guided dendrite growth into the narrow interparticle channels between SiO_2 NPs, thereby hindering penetration through the separator (Figure 7e–g).

In addition, reducible nanosized ceramic oxides, such as SiO_2, can chemically react with Li metal at dendrite tips, leading to partial etching and thereby retarding further dendritic growth [126, 128, 129]. Beyond this reactive behavior, these inorganic nanomaterials also act as stable lithiophilic species, in which polar surface oxygen groups facilitate Li^+ ion transport and enhance electrolyte wettability at the separator interface. Building upon these attributes, Park et al. recently reported a functional separator coated with nonstoichiometric SiO_2 NPs, where Si nanodots continuously scavenge Li dendrites while the surrounding SiO_2 matrix regulates Li^+ ion transport and stabilizes interfacial lithiation, collectively suppressing dendritic growth and enhancing the cycling stability of LMBs (Figure 7h) [130]. In this architecture, the highly reactive Si nanodots anchored on the SiO_2 surface effectively mitigate uncontrollable dendrite propagation *via* continuous Li consumption, whereas the SiO_2 matrix ensures the structural integrity and delays the direct dendrite penetration into the separator. The chemically stable SiO_2 component also moderates excessive lithiation of Si, thereby maintaining an optimal balance between reactivity and interfacial durability. As a result, the SiO_x-coated polyethylene (SiO_x@PE) separator enabled stable cycling for 500 hr at 1 mA cm^{-2} and 1 mAh cm^{-2} in Li||Li symmetric cells, and delivered 152 mAh g^{-1} at 5.0C with markedly enhanced capacity retention in Li||NCM811 full cells (Figure 7i–k).

While the incorporation of inorganic NPs onto the separator significantly enhances its mechanical robustness, the presence of numerous interparticle boundaries can inadvertently form preferential pathways for Li dendrite propagation, ultimately leading to internal short-circuit failure. This phenomenon similarly accounts for the vulnerability of Li garnet-based solid electrolytes, which, despite possessing a high shear modulus, remain susceptible to dendrite penetration through grain boundaries [131–133]. Therefore, proactive control of Li deposition behavior at the initial nucleation stage is essential to minimize the dendrite propagation through such structural defects.

4.2 | Chemical Modification with Lithiophilic Functionality

Given that Li dendrite formation is fundamentally driven by heterogeneous Li^+ ion transport at the electrode/separator (or

the symmetric cells with bare PP separator and ArMT@PP separators at 1 mA cm^{-2} and 1 mAh cm^{-2}, insets show enlarged views at different cycles. Reproduced with permission.[140] Copyright 2025, Wiley-VCH. (f) Cycling performance and coulombic efficiency of asymmetric Li||LFP full cells with ArMT@PP separator at 1 C. Reproduced with permission.[140] Copyright 2025, Wiley-VCH. (g) SEM image of the as-spun composite nanofiber membrane of Ag-PCNFs. Reproduced with permission.[146] Copyright 2019, American Chemical Society. (h) TEM image of Ag-PCNFs. Reproduced with permission.[146] Copyright 2019, American Chemical Society. (i) SEM image of uniform Li deposition on Ag-PCNFs from a symmetric cell after 5 cycles at 0.5 mA cm^{-2} and 0.5 mA h cm^{-2}. Reproduced with permission.[146] Copyright 2019, American Chemical Society. (j) Schematic illustration of the uniform Li deposition process on Ag-PCNFs. Reproduced with permission.[146] Copyright 2019, American Chemical Society.

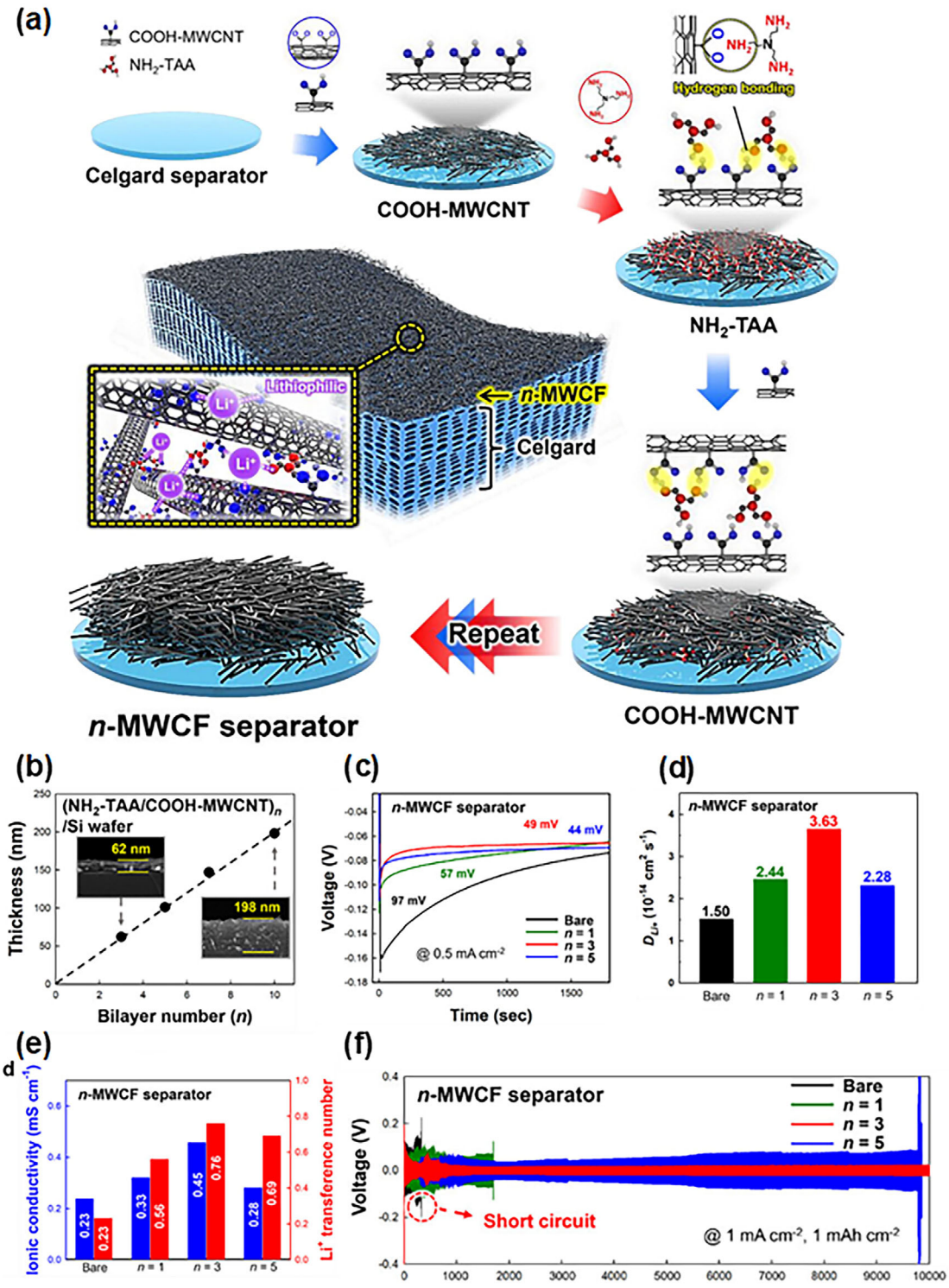

FIGURE 9 | (a) Schematic illustration for the preparation of MWCF-coated separator. Reproduced with permission.[153] Copyright 2025, Wiley-VCH. (b) Bilayer number(n)-dependent film thickness of $(NH_2\text{-TAA/COOH-MWCNT})_n$ multilayers. Insets indicate the cross-sectional SEM images. Reproduced with permission.[153] Copyright 2025, Wiley-VCH. (c) Voltage profiles of half cells with bare separator and n−MWCF separators ($n = 1, 3, 5$) during the initial Li plating at 0.5 mA cm^{-2}. Reproduced with permission.[153] Copyright 2025, Wiley-VCH. (d) Diffusion coefficient (D_{Li+}) half cells with bare separator and n−MWCF separators ($n = 1, 3, 5$). Reproduced with permission.[153] Copyright 2025, Wiley-VCH. (e) Ionic conductivity and Li^+ transference number of symmetric cells with bare separator and n−MWCF separators ($n = 1, 3, 5$). Reproduced with permission.[153] Copyright 2025, Wiley-VCH. (f) Cycling performance of symmetric cells with with bare separator and n−MWCF separators ($n = 1, 3, 5$) at 1 mA cm^{-2} and 1 mAh cm^{-2}. Reproduced with permission.[153] Copyright 2025, Wiley-VCH.

electrolyte) interface and the accompanying stochastic nucleation, the separator plays a pivotal role in stabilizing Li deposition by homogenizing ionic flux and introducing lithiophilic sites for controlled nucleation [134, 135]. Unlike purely physical blocking strategies, chemical modification that imparts lithiophilic property to the separator offers a more effective route to regulate initial Li nucleation and growth.

Among various lithiophilic materials, conjugated polymers have attracted considerable attention owing to their molecular tunability, which enables control over electronic properties and incorporation of lithiophilic functional moieties [136–139]. Recently, Yang et al. reported a donor-acceptor polymer (ArMT)—composed of benzene rings and lithiophilic triazine units—onto a polypropylene separator (ArMT@PP) *via* a simple blade-coating process to stabilize the Li anode surface (Figure 8a) [140]. The well-defined porous framework with a uniform pore size distribution mitigated localized ion accumulation, while the triazine groups reduced the Li^+ transport energy barrier, thereby improving ionic conductivity and enabling uniform Li electrodeposition during plating and stripping (Figure 8b–d). These features also facilitated the formation of a stable LiF-rich SEI film, enabling long-term cycling for 800 h in Li|ArMT@PP|Li symmetric cells (1 mA cm^{-2} and 1 mAh cm^{-2}) and delivering 127.3 mAh g^{-1} after 1200 cycles at 1C in $LiFePO_4$|ArMT@PP|Li full cells (Figure 8e,f).

During electrodeposition, Li atoms preferentially nucleate at lithiophilic sites, where the local nucleation barrier is lower. This phase transformation is governed by the direct electrochemical reduction of Li^+ ions upon electron contact [141]. Accordingly, the electrical conductivity of the lithiophilic interlayer coated on the separator becomes a crucial factor in minimizing interfacial resistance and overpotential, thereby promoting uniform Li deposition. In this regard, carbon-based materials such as CNTs and carbon nanofibers (CNF) have emerged as promising interlayer candidates due to their good electrical conductivity, mechanical robustness, and highly porous 3D architecture, which together facilitates rapid Li^+ ion transport. However, pristine carbon materials possess inert graphitic surfaces that are intrinsically lithiophobic, limiting uniform nucleation [142]. Thus, surface functionalization or hybridization with lithiophilic species is often required to fully exploit their structural and conductive advantages for dendrite suppression [143–145]. For example, Liu et al. fabricated a lithiophilic separator by coating Ag NP-embedded 3D porous CNFs onto a commercial polypropylene separator (Ag-PCNF-PP) (Figure 8g,h) [146]. The uniformly decorated Ag NPs across both the inner and outer surfaces of the PCNF scaffold offered abundant lithiophilic nucleation sites [147, 148], while the conductive carbon framework provided continuous electron pathways, ensuring smooth and homogeneous Li plating (Figure 8i,j).

Similarly, the incorporation of lithiophilic functional groups, such as hydroxyl or nitrogen-containing moieties, onto carbon interlayers has been demonstrated as an effective strategy to rationally tailoring surface chemistry [149–151]. The covalently anchored groups form a stable and homogeneously distributed lithiophilic network within the porous architecture, which not only lowers the Li nucleation barrier but also maintains long-term durability without particle coalescence or detachment during cycling [152]. Furthermore, such functional groups can act as coordination or binding sites for anchoring functional inorganic nanoparticles or establishing stable interfacial interactions with adjacent moieties. In a recent study, the Cho group reported the fabrication of an ultrathin (~62 nm-thick), lithiophilic interlayer on a commercial polypropylene separator *via* LbL assembly of carboxylic acid-functionalized multiwalled CNTs (COOH-MWCNTs) and amine-functionalized small molecule linker, tris(2-aminoethyl) amine (NH_2-TAA) (Figure 9a) [153]. Strong hydrogen-bonding interactions between each lithiophilic component and between the interlayer and separator ensured excellent structural integrity during repeated cycling. Moreover, the highly porous CNT network, uniformly decorated with dense lithiophilic sites, provided sufficient space for Li accommodation, effectively directing Li growth toward the anode surface and suppressing dendrite penetration into the separator. Given that the charge-transport kinetics at the interfaces are determinant factors in the energy density and efficiency of rechargeable battery systems, the physical characteristics of interlayer—including thickness, porosity, and uniformity, which are closely related to the interfacial resistance—must be carefully considered [154–156]. The experimental results clearly demonstrated that Li^+ ion transport and deposition behavior can be precisely controlled even within several tens of nanometers of interlayer thickness (Figure 9b–e) [153], underscoring the limitations of thick interlayers composed of polymers or carbons typically fabricated by slurry casting or vacuum filtration [140, 157]. As a result, the LbL-assembled MWCNT forest (3-MWCF)-coated separator enabled excellent long-term cycling stability for 10 000 h at 1 mA cm^{-2} and 1 mAh cm^{-2} in the Li|Li symmetric cells (Figure 9f). A quantitative comparison of representative separator-modification strategies and their electrochemical performance is summarized (Table 3), while the corresponding systematic comparisons are summarized (Table 4).

5 | Conclusion and Outlook

In summary, extensive efforts have been directed toward suppressing Li dendrite growth and stabilizing LMAs through electrolyte engineering, artificial interphase design, host electrode modification, separator functionalization, and interfacial interaction–driven assemblies. Among these, molecularly tailored interfacial strategies—including LbL assembly of lithiophilic components (e.g., COOH-, NH2-functionalized components, and/or lithiophilic metal–organic frame components) on separators or host electrodes—are particularly promising because they enable binder-free, ultrathin, and conformal interfaces with nanoscale control over thickness, composition, and uniformity. Such architectures homogenize Li^+ nucleation and ion-flux distribution and promote robust, inorganic-rich SEI formation, thereby mitigating dendritic growth while preserving porosity and minimizing inactive mass/volume penalties to support high energy density.

Importantly, this precise interfacial engineering effectively stabilizes the electrode surface without compromising the geometric features or intrinsic performance of the electrode components. Recently, numerous studies have focused on thin LMAs to

TABLE 3 | Electrochemical performance comparison of the reported separators in LMA.

Material	Method	Thickness	Symmetric cell performance	Asymmetric full cell performance	References
Formation of physical barrier					
SiO_2 (or polystyrene) NP arrays	Slurry-based Spin-coating	~1 μm	~400 h @ 3 mA cm^{-2}/3 mAh cm^{-2}	150 cycles @ 1C ($LiFePO_4$)	[127]
n-SiO_2	Slurry-based blade-coating	~3 μm	500 h @ 1 mA cm^{-2}/1 mAh cm^{-2}	~320 cycles @ 1 C ~200 mAh g^{-1} @ 0.2 C (NCM811)	[130]
$Mg(OH)_2$@MgO	Slurry coating	~2 μm	~1000 cycles @ 2 mA cm^{-2}/2 mAh cm^{-2}	~200 cycles @ 0.3 C (NCM811)	[160]
PDA@AIN[a]	Slurry coating	~18 μm	2000 h @ 1 mA cm^{-2}/1 mAh cm^{-2}	500 cycles @ 1 C 115.7 mAh g^{-1} @ 1 C ($LiFePO_4$)	[161]
Chemical modification					
ArMT (donor-acceptor polymer)	Blade-coating	~25 μm	800 h @ 1 mA cm^{-2}/1 mAh cm^{-2}	1200 cycles @ 1C 127.3 mAh g^{-1} @ 1 C ($LiFePO_4$)	[140]
Ag NP-embedded CNF[b]	EBS[c] and Knife-coating	3 μm	1500 h @ 2 mA cm^{-2}/2 mAh cm^{-2}	600 cycles @ 0.5 C 749.2 mAh g^{-1} (~77%) (sulfur)	[146]
Crosslinked pressure-sensitive adhesive (70cPSA)	Radical copolymerization	~4 μm	2500 h @ 1 mA cm^{-2}/1 mAh cm^{-2}	250 cycles @ 1 C ($LiFePO_4$)	[162]
COF nanosheet	vacuum filtration	200nm	2600 h @ 5 mA cm^{-2} / 1 mAh cm^{-2}	300 cycles @ 1C ($LiFePO_4$)	[163]
proton-doped polyaniline (PANi) nanosheets	Slurry – Blade coating	~3μm	2400 h @ 1 mA cm^{-2} / 1 mAh cm^{-2}	200 cycles @ 3C ($LiFePO_4$)	[164]
silver-nanocrystal decorated polyimide microsphere (PI@Ag microsphere)	Slurry – Blade coating	7μm	2000 h @ 1 mA cm^{-2} / 1 mAh cm^{-2}	400 cycles @1C ($LiFePO_4$)	[165]
Multiwalled CNT forest (MWCF)	Layer-by-layer assembly	~62 nm	~10 000 h @ 1 mA cm^{-2}/1 mAh cm^{-2}	1570 cycles @ 1C ($LiFePO_4$)	[153]

[a]PDA@AIN: aluminum nitride (AIN) coating on polydopamine (PDA);
[b]CNF: carbon nanofiber;
[c]EBS: electro-blown spinning.

minimize inactive weight and volume while revealing their 'true' electrochemical performance under low N/P ratio conditions. Although the adoption of thin Li foils is essential for bridging the gap between lab-scale research and commercial viability, it inevitably exposes the intrinsic instabilities of the Li metal interface, most notably Li inventory depletion and heightened geometric sensitivity [158, 159].

In this regard, molecular-level control of interfacial architectures via the LbL deposition technique—based on strong interfacial interactions—offers a rational solution as it enables the construction of conformal, ultrathin (ideally ≤100 nm) lithiophilic interlayers across complex electrode geometries. In contrast to conventional slurry-cast lithiophilic coatings with thickness ranging from several to tens of micrometers, such ultrathin interlayers homogenize interfacial Li^+ flux, suppress local current amplification, and mitigate parasitic reactions that drive inventory depletion and geometric instability. Consequently, independent of the specific fabrication route, achieving an ultrathin and highly uniform lithiophilic coating at electrode interfaces emerges as a decisive requirement for developing practical and impactful strategies toward superior electrochemical performance.

TABLE 4 | Systematic comparison of the reported separators in LMA.

Material	Method	Action Mechanism	Key Advantage	Limitation	References
Formation of physical barrier					
SiO_2 (or polystyrene) NP arrays	Slurry-based Spin-coating	Mechanical deflection	Chemistry-agnostic compatibility	Non-preventive suppression	[127]
n-SiO_2	Slurry-based blade-coating	Solvation structure modulation	Simultaneous formation and growth suppression	Initial Li consumption	[130]
$Mg(OH)_2$@MgO	Slurry coating	Reactive ion redistribution	Dendrite elimination	Initial Li consumption	[160]
PDA@AIN[a]	Slurry coating	Coordination-enabled flux homogenization	Kinetics–mechanics synergy	Structural complexity	[161]
Chemical modification					
ArMT (donor-acceptor polymer)	Blade-coating	Interfacial field regulation	Accelerated ion transport	Limited mechanical buffering	[140]
Ag NP-embedded CNF[b]	EBS[c] and Knife-coating	Lithiophilic nucleation guidance	Reversible Li utilization	Interfacial metal migration	[146]
Crosslinked pressure-sensitive adhesive (70cPSA)	Radical copolymerization	Adhesive interfacial regulation	Deformation-tolerant stability	Thickness trade-off	[162]
COF nanosheet	vacuum filtration	Anion-fixed ion sieving	Ultrathin single-ion conduction	Electrolyte-specific chemistry	[163]
proton-doped polyaniline (PANi) nanosheets	Slurry – Blade coating	Ion-flux homogenization	High-rate stability	Polymer-dependent optimization	[164]
silver-nanocrystal decorated polyimide microsphere (PI@Ag microsphere)	Slurry – Blade coating	Lithiophilic nucleation guidance	Reduced nucleation overpotential	Interfacial metal migration	[165]
Multiwalled CNT forest (MWCF)	Layer-by-layer assembly	Directed dendrite growth suppression	Gapless Ultrathin conductive layer	Time consuming	[153]

[a]PDA@AIN: aluminum nitride (AIN) coating on polydopamine (PDA);
[b]CNF: carbon nanofiber;
[c]EBS: electro-blown spinning.

Although LbL assembly-based engineering can provide the molecular-level tunability necessary for dual interfacial coordination, its practical commercialization will depend on improving fabrication time efficiency and reproducibility. To facilitate commercial adoption, the inherently time-intensive dip-based protocols should be transformed into high-speed and large-area coating platforms—such as roll-to-roll continuous processing and spray (or slot-die) deposition—thereby enhancing processing speed, coating uniformity, and batch-to-batch reproducibility. Successful integration of these manufacturing-friendly approaches would, in turn, allow the precision inherent to LbL assembly to be effectively implemented in practical devices by simultaneously ensuring (i) long-term mechanical robustness and chemical compatibility of dual lithiophilic interfaces with targeted electrolyte systems and (ii) scalable manufacturing pathways compatible with realistic cell formats.

Notably, these continuous deposition strategies are particularly well-suited for dual lithiophilic interface engineering that requires the concurrent modification of both electrodes and separators. By contrast, conventional slurry casting methods are often impractical for such applications due to limitations in thickness control, pore blockage, and poor conformality on various 3D substrates, including porous substrates. Overall, coupling LbL assembly-based interfacial chemistry with scalable coating lines can offer a direct route to preserve molecular-level tunability while satisfying the requirements of durable, reproducible, and large-area manufacturing.

Author Contributions

C.L, B.K, H.H, Y.K., and J.C. wrote and revised the manuscript. All authors discussed the results and commented on the manuscript.

Acknowledgements

This work was supported by a National Research Foundation (NRF) grant funded by the Ministry of Science, ICT & Future Planning (MSIP) (RS-2025-02214734; RS-2025-25413074), and DGIST R&D Programs of the Ministry of Science and ICT of Korea (25-ET-01).

Conflicts of Interest

The authors declare no conflict of interest.

References

1. J. Bae, K. Choi, J. Y. Cheong, et al., "Emerging Surface Engineering Methods for Lithium Metal Anodes: Critical Review Beyond Conventional SEI and Surface Coatings," *Advanced Materials* 37 (2025): 2501959.

2. B. Acebedo, M. C. Morant-Miñana, E. Gonzalo, et al., "Current Status and Future Perspective on Lithium Metal Anode Production Methods," *Advanced Energy Materials* 13 (2023): 2203744.

3. W.-J. Kwak and D. S. Rosy, "Lithium–oxygen Batteries and Related Systems: Potential, Status, and Future," *Chemical Reviews* 120 (2020): 6626–6683.

4. L.-P. Hou, X.-Q. Zhang, B.-Q. Li, and Q. Zhang, "Challenges and Promises of Lithium Metal Anode by Soluble Polysulfides in Practical Lithium–sulfur Batteries," *Materials Today* 45 (2021): 62–76.

5. L. Lin, H. Zheng, Q. Luo, et al., "Regulating Lithium Nucleation at the Electrolyte/Electrode Interface in Lithium Metal Batteries," *Advanced Functional Materials* 34 (2024): 2315201.

6. X.-B. Cheng, R. Zhang, C.-Z. Zhao, et al., "A Review of Solid Electrolyte Interphases on Lithium Metal Anode," 3 (2016): 1500213.

7. Y. Chen, Y. Luo, H. Zhang, et al., "The Challenge of Lithium Metal Anodes for Practical Applications," *Small Methods* 3 (2019): 1800551.

8. L. Wang, Z. Zhou, X. Yan, et al., "Engineering of Lithium-Metal Anodes Towards a Safe and Stable Battery," *Energy Storage Materials* 14 (2018): 22–48.

9. Z. A. Ghazi, Z. Sun, C. Sun, et al., "Key Aspects of Lithium Metal Anodes for Lithium Metal Batteries," *Small* 15 (2019): 1900687.

10. X. He, K. Zhang, Z. Zhu, Z. Tong, and X. Liang, "3D-Hosted Lithium Metal Anodes," *Chemical Society Reviews* 53 (2024): 9–24.

11. Y. Zhang, M. Yao, T. Wang, H. Wu, and Y. Zhang, "A 3D Hierarchical Host with Gradient-distributed Dielectric Properties Toward Dendrite-free Lithium Metal Anode," *Angewandte Chemie* 136 (2024): 202403399.

12. J. Seo, J. Im, M. Kim, et al., "Recent Progress of Advanced Functional Separators in Lithium Metal Batteries," *Small* 20 (2024): 2312132.

13. L. Cao, Y. Deng, S. Zhang, et al., "Separators for Rechargeable Metal Batteries: Design Principles and Evaluation," *Advanced Functional Materials* 35 (2025): 2425517.

14. C. Wang, X. Fu, C. Ying, J. Liu, and W.-H. Zhong, "Natural Protein as Novel Additive of a Commercial Electrolyte for Long-Cycling Lithium Metal Batteries," *Chemical Engineering Journal* 437 (2022): 135283.

15. O. B. Chae and B. L. Lucht, "Interfacial Issues and Modification of Solid Electrolyte Interphase for Li Metal Anode in Liquid and Solid Electrolytes," *Advanced Energy Materials* 13 (2023): 2203791.

16. B. Peng, W. Zhang, J. Du, et al., "Decoupling Electronic and Ionic Conductivities of Electrochemically Active $LiCoO_2$ as Solid-State Electrolyte for Li Metal Batteries," *Advanced Functional Materials* 36 (2025): 14420.

17. X. Xiong, S. Xu, W. Zhang, et al., "A Thioether Additive as Interfacial Regulator for Ultra-stable Lithium Metal Batteries," *National Science Review* 12 (2025): nwaf259.

18. P. Zhai, L. Liu, X. Gu, et al., "Interface Engineering for Lithium Metal Anodes in Liquid Electrolyte," *Advanced Energy Materials* 10 (2020): 2001257.

19. Q. Yan, G. Whang, Z. Wei, et al., "A Perspective on Interfacial Engineering of Lithium Metal Anodes and Beyond," *Applied Physics Letters* 117 (2020).

20. G. Lu, J. Nai, D. Luan, et al., "Surface Engineering Toward Stable Lithium Metal Anodes," *Science Advances* 9 (2023): adf1550.

21. Z. Li, W. Ji, T. X. Wang, et al., "Maximized Lithiophilic Carbonyl Units in Covalent Organic Frameworks as Effective Li ion Regulators for Lithium Metal Batteries," *Chemical Engineering Journal* 437 (2022): 135293.

22. J. Zhao, G. Yan, and X. Zhang, "In situ Interfacial Polymerization of Lithiophilic COF@ PP and POP@ PP Separators with Lower Shuttle Effect and Higher ion Transport for High-performance Li–S Batteries," *Chemical Engineering Journal* 442 (2022): 136352.

23. Y. Wang, H. Hou, K. Tantratian, et al., "Insight into the Interface Design for Li Metal Anode: Organic-Rich or Inorganic-Rich," *Advanced Functional Materials* 34 (2024): 2406426.

24. O. Borodin and G. D. Smith, "Quantum Chemistry and Molecular Dynamics Simulation Study of Dimethyl Carbonate: Ethylene Carbonate Electrolytes Doped with $LiPF_6$," *The Journal of Physical Chemistry B* 113 (2009): 1763–1776.

25. X. Bogle, R. Vazquez, S. Greenbaum, et al., "Understanding Li^+–solvent Interaction in Nonaqueous Carbonate Electrolytes with ^{17}O NMR," *The Journal of Physical Chemistry Letters* 4 (2013): 1664–1668.

26. Y. Liu, Q. Liu, L. Xin, et al., "Making Li-metal Electrodes Rechargeable by Controlling the Dendrite Growth Direction," *Nature Energy* 2 (2017): 1–10.

27. J. Ding, T. Du, L. R. Jensen, et al., "High-Performance Dendrite-Free Lithium Metal Anode Based on Metal-Organic Framework Glass," *Advanced Materials* 36 (2024): 2400652.

28. Y. Li, H. Xu, Q. Ning, et al., "Visualizing Structure, Growth, and Dynamics of Li dendrite in Batteries: From Atomic to Device Scales," *Advanced Functional Materials* 34 (2024): 2401361.

29. C. Monroe and J. Newman, "Dendrite Growth in Lithium/Polymer Systems: A Propagation Model for Liquid Electrolytes Under Galvanostatic Conditions," *Journal of The Electrochemical Society* 150 (2003): A1377.

30. L. He, Q. Sun, L. Lu, and S. Adams, "Understanding and Preventing Dendrite Growth in Lithium Metal Batteries," *ACS Applied Materials & Interfaces* 13 (2021): 34320–34331.

31. D. Lin, Y. Liu, and Y. Cui, "Reviving the Lithium Metal Anode for High-energy Batteries," *Nature Nanotechnology* 12 (2017): 194–206.

32. D. R. Ely and R. E. García, "Heterogeneous Nucleation and Growth of Lithium Electrodeposits on Negative Electrodes," *Journal of the Electrochemical Society* 160 (2013): A662.

33. X. Gao, Y.-N. Zhou, D. Han, et al., "Thermodynamic Understanding of Li-dendrite Formation," *Joule* 4 (2020): 1864–1879.

34. A. Jana and R. E. García, "Lithium Dendrite Growth Mechanisms in Liquid Electrolytes," *Nano Energy* 41 (2017): 552–565.

35. J. B. Park, C. Choi, S. Yu, K. Y. Chung, and D.-W. Kim, "Porous Lithiophilic Li–Si Alloy-type Interfacial Framework via Self-discharge Mechanism for Stable Lithium Metal Anode with Superior Rate," *Advanced Energy Materials* 11 (2021): 2101544.

36. A. Huang, Y. Wu, H. Huang, et al., "Lithiophilic Mo_2C Clusters-embedded Carbon Nanofibers for High Energy Density Lithium Metal Batteries," *Advanced Functional Materials* 33 (2023): 2303111.

37. W. Yao, Z. Chen, X. Zhang, et al., "Lithiophilic V_2CT_X/MoO_3 Hosts with Electronic/Ionic Dual Conductive Gradients for Ultrahigh-rate Lithium Metal Anodes," *Advanced Functional Materials* 34 (2024): 2400348.

38. X. Zhou, S. Wang, Y. Li, et al., "Boosting Li-Metal Anode Performance with Lithiophilic Li–Zn Seeds in a 2D Reduced Graphene Oxide Scaffold," *Advanced Energy Materials* 15 (2025): 2403640.

39. X. Chen, X.-R. Chen, T.-Z. Hou, et al., "Lithiophilicity Chemistry of Heteroatom-doped Carbon to Guide Uniform Lithium Nucleation in Lithium Metal Anodes," *Science Advances* 5 (2019): aau7728.

40. A. Jana, S. I. Woo, K. S. N. Vikrant, and R. E. García, "Electrochemo-mechanics of Lithium Dendrite Growth," *Energy & Environmental Science* 12 (2019): 3595–3607.

41. J. Thomas, S. S. Behara, and A. Van der Ven, "Thermodynamic and Kinetic Properties of the Lithium–silver System," *Chemistry of Materials* 36 (2024): 8936–8948.

42. J. Seo, J. Lim, H. Chang, et al., "Sustaining Surface Lithiophilicity of Ultrathin Li-Alloy Coating Layers on Current Collector for Zero-Excess Li-Metal Batteries," *Small* 20 (2024): 2402988.

43. K. Yan, Z. Lu, H.-W. Lee, et al., "Selective Deposition and Stable Encapsulation of Lithium Through Heterogeneous Seeded Growth," *Nature Energy* 1 (2016): 1–8.

44. J. Zhang, H. Chen, M. Wen, et al., "Lithiophilic 3D copper-based Magnetic Current Collector for Lithium-free Anode to Realize Deep Lithium Deposition," *Advanced Functional Materials* 32 (2022): 2110110.

45. Y. Hui, Y. Wu, W. Sun, et al., "Nanosecond Pulsed Laser-Assisted Deposition to Construct a 3D Quasi-Gradient Lithiophilic Skeleton for Stable Lithium Metal Anodes," *Advanced Functional Materials* 33 (2023): 2303319.

46. Y. Xu, K. Dong, Y. Jie, et al., "Promoting Mechanistic Understanding of Lithium Deposition and Solid-electrolyte Interphase (SEI) Formation Using Advanced Characterization and Simulation Methods: Recent Progress, Limitations, and Future Perspectives," *Advanced Energy Materials* 12 (2022): 2200398.

47. L. Song, D. Ning, Y. Chai, et al., "Correlating Solid Electrolyte Interphase Composition with Dendrite-Free and Long Life-Span Lithium Metal Batteries via Advanced Characterizations and Simulations," *Small Methods* 7 (2023): 2300168.

48. L. Fan, H. L. Zhuang, W. Zhang, et al., "Stable Lithium Electrodeposition at Ultra-high Current Densities Enabled by 3D PMF/Li Composite Anode," *Advanced Energy Materials* 8 (2018): 1703360.

49. K. Huang, Z. Li, Q. Xu, et al., "Lithiophilic CuO Nanoflowers on Ti-mesh Inducing Lithium Lateral Plating Enabling Stable Lithium-metal Anodes with Ultrahigh Rates and Ultralong Cycle Life," *Advanced Energy Materials* 9 (2019): 1900853.

50. C. Wang, A. Wang, L. Ren, et al., "Controlling Li ion Flux Through Materials Innovation for Dendrite-free Lithium Metal Anodes," *Advanced Functional Materials* 29 (2019): 1905940.

51. W. Guo, S. Liu, X. Guan, et al., "Mixed ion and Electron-conducting Scaffolds for High-rate Lithium Metal Anodes," *Advanced Energy Materials* 9 (2019): 1900193.

52. S. Ni, J. Sheng, and C. Zhang, "Dendrite-free Lithium Deposition and Stripping Regulated by Aligned Microchannels for Stable Lithium Metal Batteries," *Advanced Functional Materials* 32 (2022): 2200682.

53. L. Xu, Q. Zhang, S. Niu, et al., "Organic Eutectic Mixture Incorporated with Graphene Oxide Sheets as Lithiophilic Artificial Protective Layer for Dendrite-Free Lithium Metal Batteries," *Advanced Energy Materials* 13 (2023): 2204214.

54. Y. Gao and B. Zhang, "Probing the Mechanically Stable Solid Electrolyte Interphase and the Implications in Design Strategies," *Advanced materials* 35 (2023): 2205421.

55. J. Tan, J. Matz, P. Dong, J. Shen, and M. Ye, "A Growing Appreciation for the Role of LiF in the Solid Electrolyte Interphase," *Advanced Energy Materials* 11 (2021): 2100046.

56. Y. Li, F. Bai, C. Li, Y. Wang, and T. Li, "Understanding the Inorganic-rich Feature of Anion-derived Solid Electrolyte Interphase," *Advanced Energy Materials* 14 (2024): 2304414.

57. J. Yang, M. Li, Z. Sun, et al., "Prolonging the Cycling Lifetime of Lithium Metal Batteries with a Monolithic and Inorganic-rich Solid Electrolyte Interphase," *Energy & Environmental Science* 16 (2023): 3837–3846.

58. S. Liu, X. Ji, J. Yue, et al., "High Interfacial-energy Interphase Promoting Safe Lithium Metal Batteries," *Journal of the American Chemical Society* 142 (2020): 2438–2447.

59. H. Adenusi, G. A. Chass, S. Passerini, K. V. Tian, and G. Chen, "Lithium Batteries and the Solid Electrolyte Interphase (SEI)—Progress and Outlook," *Advanced Energy Materials* 13 (2023): 2203307.

60. F. Hao, A. Verma, and P. P. Mukherjee, "Mechanistic Insight Into Dendrite–SEI Interactions for Lithium Metal Electrodes," *Journal of Materials Chemistry A* 6 (2018): 19664–19671.

61. P. Shi, T. Li, R. Zhang, et al., "Lithiophilic LiC_6 Layers on Carbon Hosts Enabling Stable Li metal Anode in Working Batteries," *Advanced Materials* 31 (2019): 1807131.

62. T. Yang, L. Li, F. Wu, and R. Chen, "A Soft Lithiophilic Graphene Aerogel for Stable Lithium Metal Anode," *Advanced Functional Materials* 30 (2020): 2002013.

63. G. Wang, T. Liu, X. Fu, et al., "Lithiophilic Amide-Functionalized Carbon Nanotube Skeleton for Dendrite-free Lithium Metal Anodes," *Chemical Engineering Journal* 414 (2021): 128698.

64. A. Huang, H. Huang, S. Li, et al., "Conversion–Lithiophilicity Hosts Toward Long-Term and High-Energy-Density Lithium Metal Batteries," *Advanced Energy Materials* 15 (2025): 2403576.

65. Z. Yang, T. Hwang, Y. Mu, et al., "Understanding the Mechanistic Role of Reversible LiAg Alloy Interphases in Ultralong-cycle Lithium-metal Batteries," *Chemical Engineering Journal* 524 (2025): 169212.

66. F. Guo, C. Wu, H. Chen, et al., "Dendrite-free Lithium Deposition by Coating a Lithiophilic Heterogeneous Metal Layer on Lithium Metal Anode," *Energy Storage Materials* 24 (2020): 635–643.

67. B. Hong, H. Fan, X.-B. Cheng, et al., "Spatially Uniform Deposition of Lithium Metal in 3D Janus Hosts," *Energy Storage Materials* 16 (2019): 259–266.

68. M. Zhu, X. Teng, X. Li, et al., "Ameliorating Lithium Deposition Regulation Via Alloying Lithiophilic Zinc Metal for Stable Lithium Metal Batteries," *Chemical Engineering Journal* 506 (2025): 160150.

69. S. Lee, Y. Lee, W.-J. Song, et al., "Integration of Deformable Matrix and Lithiophilic Sites for Stable and Stretchable Lithium Metal Batteries," *Energy Storage Materials* 73 (2024): 103850.

70. W. Jia, J. Zhang, L. Zheng, et al., "Lithium-rich Alloy as Stable Lithium Metal Composite Anode for Lithium Batteries," 4 (2024): 100266.

71. C. Yang, Y. Yao, S. He, et al., "Ultrafine Silver Nanoparticles for Seeded Lithium Deposition Toward Stable Lithium Metal Anode," *Advanced Materials* 29 (2017): 1702714.

72. W. Chen, M. Fu, Q. Zhao, et al., "Au-modified 3D Carbon Cloth as a Dendrite-free Framework for Li Metal with Excellent Electrochemical Stability," *Journal of Alloys and Compounds* 871 (2021): 159491.

73. K. Ssendagire, I. Phiri, and S.-Y. Ryou, "Operando Characterization of Dendrite-Free Silver Nanoparticle/Lithium Metal Powder Composite Anodes," *ACS Applied Materials & Interfaces* 17 (2025): 29757–29769.

74. B. A. Korgel, S. Fullam, S. Connolly, and D. Fitzmaurice, "Assembly and Self-organization of Silver Nanocrystal Superlattices: Ordered 'Soft Spheres," *The Journal of Physical Chemistry B* 102 (1998): 8379–8388.

75. Y. Song, D. Kim, S. Kang, et al., "Room-temperature Metallic Fusion-induced Layer-by-layer Assembly for Highly Flexible Electrode Applications," *Advanced Functional Materials* 29 (2019): 1806584.

76. S. Lee, Y. Song, Y. Ko, et al., "A Metal-like Conductive Elastomer With a Hierarchical Wrinkled Structure," *Advanced Materials* 32 (2020): 1906460.

77. J. Ko, C. Kim, D. Kim, et al., "High-performance Electrified Hydrogel Actuators Based on Wrinkled Nanomembrane Electrodes for Untethered Insect-scale Soft Aquabots," *Science Robotics* 7 (2022): abo6463.

78. B. Yu, T. Tao, S. Mateti, S. Lu, and Y. Chen, "Nanoflake Arrays of Lithiophilic Metal Oxides for the Ultra-stable Anodes of Lithium-metal Batteries," *Advanced Functional Materials* 28 (2018): 1803023.

79. J. Luan, Q. Zhang, H. Yuan, et al., "Plasma-strengthened Lithiophilicity of Copper Oxide Nanosheet–decorated Cu Foil for Stable Lithium Metal Anode," *Advanced Science* 6 (2019): 1901433.

80. Z. Jiang, R. Yuan, Z. Jiang, et al., "Utilizing Ultra-homogeneous SiO_x and Defects to Achieve Interlayer Protection for Lithium Metal Anodes," *Small* 19 (2023): 2303294.

81. Y. Mei, J. Zhou, Y. Hao, et al., "High-lithiophilicity Host With Micro/Nanostructured Active Sites Based on Wenzel Wetting Model for Dendrite-free Lithium Metal Anodes," *Advanced Functional Materials* 31 (2021): 2106676.

82. W. Chen, R. V. Salvatierra, M. Ren, et al., "Laser-induced Silicon Oxide for Anode-free Lithium Metal Batteries," *Advanced Materials* 32 (2020): 2002850.

83. X. Yan, F. Ye, Y. Zhang, et al., "Understanding the Anchoring Effect on Li Plating with Indium Tin Oxide Layer Functionalized Hosts for Li metal Anodes," *Chemical Engineering Journal* 440 (2022): 135827.

84. D. Park, J. Park, and W. Choi, "Versatile Multi-lithiophilic Metal Oxide Nano Seeds Embedded in Hollow Carbon Nanospheres Via Electrostatically Functional Template for Dendrite-free Lithium Metal Anodes," *Chemical Engineering Journal* 491 (2024): 152146.

85. S.-S. Chi, Y. Liu, W.-L. Song, L.-Z. Fan, and Q. Zhang, "Prestoring Lithium Into Stable 3D Nickel foam Host as Dendrite-free Lithium Metal Anode," *Advanced Functional Materials* 27 (2017): 1700348.

86. W. Zhu, W. Deng, F. Zhao, et al., "Graphene Network Nested Cu foam for Reducing Size of Lithium Metal Towards Stable Metallic Lithium Anode," *Energy Storage Materials* 21 (2019): 107–114.

87. K. Liu, Z. Li, W. Xie, et al., "Oxygen-rich Carbon Nanotube Networks for Enhanced Lithium Metal Anode," *Energy Storage Materials* 15 (2018): 308–314.

88. F. Liu, R. Xu, Z. Hu, et al., "Regulating Lithium Nucleation via CNTs Modifying Carbon Cloth Film for Stable Li Metal Anode," *Small* 15 (2019): 1803734.

89. Z. Sun, S. Jin, H. Jin, et al., "Robust Expandable Carbon Nanotube Scaffold for Ultrahigh-capacity Lithium-metal Anodes," *Advanced Materials* 30 (2018): 1800884.

90. R. Zhang, X.-R. Chen, X. Chen, et al., "Lithiophilic Sites in Doped Graphene Guide Uniform Lithium Nucleation for Dendrite-free Lithium Metal Anodes," *Angewandte Chemie* 129 (2017): 7872–7876.

91. Z. Chen, W. Chen, H. Wang, et al., "Lithiophilic Anchor Points Enabling Endogenous Symbiotic Li_3N Interface for Homogeneous and Stable Lithium Electrodeposition," *Nano Energy* 93 (2022): 106836.

92. X.-X. Ma, X. Chen, Y.-K. Bai, et al., "The Defect Chemistry of Carbon Frameworks for Regulating the Lithium Nucleation and Growth Behaviors in Lithium Metal Anodes," *Small* 17 (2021): 2007142.

93. S. Yu, X. Yu, S. Shivakumar, et al., "Defect-mediated Faceted Lithium Nucleation on Carbon Composite Substrates," *ACS Nano* 18 (2024): 17031–17040.

94. D. Pan, C. Zhao, X. Qi, et al., "Defect-abundant Commercializable 3D Carbon Papers for Fabricating Composite Li anode with High Loading and Long Life," *Energy Storage Materials* 50 (2022): 407–416.

95. J.-K. Meng, W.-W. Wang, X.-Y. Yue, et al., "Cotton-derived Carbon Cloth Enabling Dendrite-free Li Deposition for Lithium Metal Batteries," *Journal of Power Sources* 465 (2020): 228291.

96. Y. Xie, J. Hu, Z. Han, et al., "Ultra-stable K metal Anode Enabled by Oxygen-rich Carbon Cloth," *Nano Research* 13 (2020): 3137–3141.

97. J. Bae, K. Choi, H. Song, et al., "Reinforcing Native Solid-Electrolyte Interphase Layers via Electrolyte-Swellable Soft-Scaffold for Lithium Metal Anode," *Advanced Energy Materials* 13 (2023): 2203818.

98. Q. Wang, C. Yang, J. Yang, et al., "Stable Li Metal Anode with Protected Interface for High-performance Li metal Batteries," *Energy Storage Materials* 15 (2018): 249–256.

99. C. Niu, H. Pan, W. Xu, et al., "Self-smoothing Anode for Achieving High-energy Lithium Metal Batteries Under Realistic Conditions," *Nature Nanotechnology* 14 (2019): 594–601.

100. M. Kwon, D. Nam, S. Lee, et al., "Textile-type Lithium-ion Battery Cathode Enabling High Specific/Areal Capacities and High Rate Capability Through Ligand Replacement Reaction-mediated Assembly," *Advanced Energy Materials* 11 (2021): 2101631.

101. L. Ma, Y. Nie, Y. Liu, et al., "Preparation of Core/Shell Electrically Conductive Fibers by Efficient Coating Carbon Nanotubes on Polyester," *Advanced Fiber Materials* 3 (2021): 180–191.

102. T. Zhao, G. Zhang, F. Zhou, S. Zhang, and C. Deng, "Toward Tailorable Zn-ion Textile Batteries with High Energy Density and Ultrafast Capability: Building High-Performance Textile Electrode in 3D Hierarchical Branched Design," *Small* 14 (2018): 1802320.

103. L. Allison, S. Hoxie, and T. L. Andrew, "Towards Seamlessly-integrated Textile Electronics: Methods to Coat Fabrics and Fibers with Conducting Polymers for Electronic Applications," *Chemical Communications* 53 (2017): 7182–7193.

104. Y. Ding, M. A. Invernale, and G. A. Sotzing, "Conductivity trends of PEDOT-PSS Impregnated Fabric and the Effect of Conductivity on

Electrochromic Textile," *ACS Applied Materials & Interfaces* 2 (2010): 1588–1593.

105. L. Liu, Y. Yu, C. Yan, K. Li, and Z. Zheng, "Wearable Energy-dense and Power-dense Supercapacitor Yarns Enabled by Scalable Graphene–metallic Textile Composite Electrodes," *Nature Communications* 6 (2015): 7260.

106. Y. Zhu, M. Yang, Q. Huang, et al., "V_2O_5 Textile Cathodes with High Capacity and Stability for Flexible Lithium-ion Batteries," *Advanced Materials* 32 (2020): 1906205.

107. J. Cai, L. Wang, Q. Huang, et al., "A Thin, Stable, and Flexible Janus Lithium-Textile Anode for Long-Life and High-Energy Lithium Metal Battery," *Advanced Energy Materials* 14 (2024): 2303088.

108. D. Nam, G. Yu, C. Lee, et al., "High-Performance Dendrite-Free Lithium Textile Anodes Using Interfacial Interaction-Mediated Ultrathin Metal Organic Framework Multilayers," *Advanced Materials* 38 (2025): 08218.

109. Z. Tong, B. Bazri, S. F. Hu, et al., "Interfacial Chemistry in Anode-free Batteries: Challenges and Strategies," *Journal of Materials Chemistry A* 9 (2021): 7396–7406.

110. S. S. Zhang, "A Review on the Separators of Liquid Electrolyte Li-ion Batteries," *Journal of power sources* 164 (2007): 351–364.

111. H. Lee, M. Yanilmaz, O. Toprakci, K. Fu, and X. Zhang, "A Review of Recent Developments in Membrane Separators for Rechargeable Lithium-ion Batteries," *Energy & Environmental Science* 7 (2014): 3857–3886.

112. C. F. J. Francis, I. L. Kyratzis, and A. S. Best, "Lithium-ion Battery Separators for Ionic-liquid Electrolytes: A Review," *Advanced Materials* 32 (2020): 1904205.

113. Z. Fan, X. Chen, J. Shi, et al., "Functionalized Separators Boosting Electrochemical Performances for Lithium Batteries," *Nano-Micro Letters* 17 (2025): 128.

114. D. Wang, W. Zhang, W. Zheng, et al., "Towards High-safe Lithium Metal Anodes: Suppressing Lithium Dendrites via Tuning Surface Energy," 4 (2017): 1600168.

115. J. Pu, J. Li, K. Zhang, et al., "Conductivity and Lithiophilicity Gradients Guide Lithium Deposition to Mitigate Short Circuits," *Nature Communications* 10 (2019): 1896.

116. Y. Liu, J. Sun, X. Hu, et al., "Lithiophilic Sites Dependency of Lithium Deposition in Li metal Host Anodes," *Nano Energy* 94 (2022): 106883.

117. A. Masias, N. Felten, R. Garcia-Mendez, J. Wolfenstine, and J. Sakamoto, "Elastic, Plastic, and Creep Mechanical Properties of Lithium Metal," *Journal of Materials Science* 54 (2019): 2585–2600.

118. Y. Li, Y. Li, A. Pei, et al., "Atomic Structure of Sensitive Battery Materials and Interfaces Revealed by Cryo–electron Microscopy," *Science* 358 (2017): 506–510.

119. X.-R. Chen, B.-C. Zhao, C. Yan, and Q. Zhang, "Review on Li deposition in Working Batteries: From Nucleation to Early Growth," *Advanced Materials* 33 (2021): 2004128.

120. C. Xu, Z. Ahmad, A. Aryanfar, V. Viswanathan, and J. R. Greer, "Enhanced Strength and Temperature Dependence of Mechanical Properties of Li at Small Scales and Its Implications for Li Metal Anodes," *Proceedings of the National Academy of Sciences* 114 (2017): 57–61.

121. L. Zhang, T. Yang, C. Du, et al., "Lithium Whisker Growth and Stress Generation in an In situ Atomic Force Microscope–environmental Transmission Electron Microscope Set-up," *Nature Nanotechnology* 15 (2020): 94–98.

122. P. Wange, T. Höche, C. Rüssel, and J. D. Schnapp, "Microstructure-property Relationship in High-strength $MgO–Al_2O_3–SiO_2–TiO_2$ Glass-ceramics," *Journal of Non-Crystalline Solids* 298 (2002): 137–145.

123. M. Yanilmaz, Y. Lu, Y. Li, and X. Zhang, "SiO_2/Polyacrylonitrile Membranes via Centrifugal Spinning as a Separator for Li-ion Batteries," *Journal of Power Sources* 273 (2015): 1114–1119.

124. D. Parikh, C. J. Jafta, B. P. Thapaliya, et al., "Al_2O_3/TiO_2 Coated Separators: Roll-to-roll Processing and Implications for Improved Battery Safety and Performance," *Journal of Power Sources* 507 (2021): 230259.

125. K. Liu, D. Zhuo, H.-W. Lee, et al., "Extending the Life of Lithium-based Rechargeable Batteries by Reaction of Lithium Dendrites with a Novel Silica Nanoparticle Sandwiched Separator," *Advanced Materials* 29 (2016): 1603987.

126. J. Park, Y. J. Kwon, J. Yun, et al., "Ultra-thin SiO_2 Nanoparticle Layered Separators by a Surface Multi-functionalization Strategy for Li-metal Batteries: Highly Enhanced Li-dendrite Resistance and Thermal Properties," *Energy Storage Materials* 65 (2024): 103135.

127. J. Liang, Q. Chen, X. Liao, et al., "A Nano-shield Design for Separators to Resist Dendrite Formation in Lithium-metal Batteries," *Angewandte Chemie International Edition* 59 (2020): 6561–6566.

128. R. Pathak, K. Chen, A. Gurung, et al., "Ultrathin Bilayer of Graphite/SiO_2 as Solid Interface for Reviving Li Metal Anode," *Advanced Energy Materials* 9 (2019): 1901486.

129. P. Xue, C. Sun, H. Li, J. Liang, and C. Lai, "Superlithiophilic Amorphous $SiO_2–TiO_2$ Distributed into Porous Carbon Skeleton Enabling Uniform Lithium Deposition for Stable Lithium Metal Batteries," *Advanced Science* 6 (2019): 1900943.

130. B. K. Park, D. W. Nam, D. Ma, et al., "Strategic Design of a Functional Separator with Dual-Acting Si/SiO_x Nanocomposite for Dendrite-Free Li–Metal Batteries," *ACS Nano* 19 (2025): 26659–26672.

131. Y. Ren, Y. Shen, Y. Lin, and C.-W. Nan, "Direct Observation of Lithium Dendrites Inside Garnet-type Lithium-ion Solid Electrolyte," *Electrochemistry Communications* 57 (2015): 27–30.

132. C. Zhu, T. Fuchs, S. A. L. Weber, et al., "Understanding the Evolution of Lithium Dendrites at $Li_{6.25}Al_{0.25}La_3Zr_2O_{12}$ Grain Boundaries via Operando Microscopy Techniques," *Nature Communications* 14 (2023): 1300.

133. C. Yuan, X. Gao, Y. Jia, et al., "Coupled Crack Propagation and Dendrite Growth in Solid Electrolyte of All-solid-state Battery," *Nano Energy* 86 (2021): 106057.

134. X. Zhang, A. Wang, X. Liu, and J. Luo, "Dendrites in Lithium Metal Anodes: Suppression, Regulation, and Elimination," *Accounts of Chemical Research* 52 (2019): 3223–3232.

135. Y. Ji, L. Dong, J. Liu, et al., "A Li^+-flux-Homogenizing Separator for Long-term Cycling of Li Metal Anodes," *Energy & Environmental Science* 17 (2024): 4078–4089.

136. K. Wang, T. Zhao, R. Lv, et al., "Dendrite-free Lithium-metal Batteries Enabled by 2D Lithophilic Conjugated Polymer on Separator," *Advanced Energy Materials* 14 (2024): 2401281.

137. Y. Yang, P. Mu, B. Li, A. Li, and J. Zhang, "In situ Separator Modification with an N-rich Conjugated Microporous Polymer for the Effective Suppression of Polysulfide Shuttle and Li dendrite Growth," *ACS Applied Materials & Interfaces* 14 (2022): 49224–49232.

138. Z. Wang, R. Pan, C. Xu, et al., "Conducting Polymer Paper-derived Separators for Lithium Metal Batteries," *Energy Storage Materials* 13 (2018): 283–292.

139. W. Liu, K. Zhang, L. Ma, et al., "An ion Sieving Conjugated Microporous Thermoset Ultrathin Membrane for High-performance Li-S Battery," *Energy Storage Materials* 49 (2022): 1–10.

140. T. Yang, X. Xu, S. Chen, et al., "A Lithiophilic Donor–Acceptor Polymer Modified Separator for High-Performance Lithium Metal Batteries," *Angewandte Chemie* 137 (2025): 202420973.

141. B. Thirumalraj, T. T. Hagos, C.-J. Huang, et al., "Nucleation and Growth Mechanism of Lithium Metal Electroplating," *Journal of the American Chemical Society* 141 (2019): 18612–18623.

142. J. Noh, J. Tan, D. R. Yadav, et al., "Understanding of Lithium Insertion into 3D Porous Carbon Scaffolds with Hybridized Lithiophobic

and Lithiophilic Surfaces by In-operando Study," *Nano Letters* 20 (2020): 3681–3687.

143. W. Ouyang, H. Tan, X. Liu, et al., "Ag Nanoparticles Decorated N-Doped Carbon Fiber as 3D Host for Robust Li Metal Anode," *ACS Applied Energy Materials* 8 (2025): 9101–9109.

144. H. Zhang, X. Liao, Y. Guan, et al., "Lithiophilic-lithiophobic Gradient Interfacial Layer for a Highly Stable Lithium Metal Anode," *Nature Communications* 9 (2018): 3729.

145. C. Zheng, S. Y. Sayed, C. W. Reese, et al., "Enhancing Lithium Metal Anode Stability through Surface Modification and Heat Treatment for 3D Current Collectors," *ACS Applied Materials & Interfaces* 17 (2025): 44333–44346.

146. M. Liu, N. Deng, J. Ju, et al., "Silver Nanoparticle-doped 3D Porous Carbon Nanofibers as Separator Coating for Stable Lithium Metal Anodes," *ACS Applied Materials & Interfaces* 11 (2019): 17843–17852.

147. R. Zhang, X. Chen, X. Shen, et al., "Coralloid Carbon Fiber-based Composite Lithium Anode for Robust Lithium Metal Batteries," 2 (2018): 764–777.

148. Y. Wang, Z. Jiang, Y. Li, et al., "Functional Ag-$C_3N_{4\cdot5}$ Composite Nanoribbon-Coated Separator Suppresses Lithium Dendrite Growth," *Journal of Alloys and Compounds* 1047 (2025): 185090.

149. H. Jia, J. Fan, P. Su, T. Guo, and M.-C. Liu, "Cobalt Nitride Nanoparticles Encapsulated in N-Doped Carbon Nanotubes Modified Separator of Li–S Battery Achieving the Synergistic Effect of Restriction-Adsorption-Catalysis of Polysulfides," *Small* 20 (2024): 2311343.

150. W.-K. Shin, A. G. Kannan, and D.-W. Kim, "Effective Suppression of Dendritic Lithium Growth Using an Ultrathin Coating of Nitrogen and Sulfur Codoped Graphene Nanosheets on Polymer Separator for Lithium Metal Batteries," *ACS Applied Materials & Interfaces* 7 (2015): 23700–23707.

151. K. M. Yang, K. Yang, M. Cho, S. Kim, and Y. LEE, "Self-assembled Functional Layers onto Separator Toward Practical Lithium Metal Batteries," *Chemical Engineering Journal* 454 (2023): 140191.

152. J. Sun, Y. Cheng, H. Zhang, et al., "Enhanced Cyclability of Lithium Metal Anodes Enabled by Anti-aggregation of Lithiophilic Seeds," *Nano Letters* 22 (2022): 5874–5882.

153. D. Nam, K. Jin, T. H. Jo, et al., "Ultrathin, Layer-by-Layer Assembled Lithiophilic Interlayers for Dendritic Growth-Suppressed Lithium Metal Anodes," *Advanced Energy Materials* 15 (2025): 2500850.

154. H. Qian, X. Li, Q. Chen, et al., "LiZn/Li_2O Induced Chemical Confinement Enabling Dendrite-free Li-metal Anode," *Advanced Functional Materials* 34 (2024): 2310143.

155. S. Zhou, P. Huang, T. Xiong, et al., "Sub-thick Electrodes with Enhanced Transport Kinetics via in situ Epitaxial Heterogeneous Interfaces for High Areal-capacity Lithium Ion Batteries," *Small* 17 (2021): 2100778.

156. Z. Chen, D. L. Danilov, R.-A. Eichel, and P. H. L. Notten, "Porous Electrode Modeling and its Applications to Li-ion Batteries," *Advanced Energy Materials* 12 (2022): 2201506.

157. R. Pan, R. Sun, Z. Wang, et al., "Double-sided Conductive Separators for Lithium-metal Batteries," *Energy Storage Materials* 21 (2019): 464–473.

158. L. Wichmann, S. K. Jiang, J. H. Thienenkamp, et al., "Origins of Lithium Inventory Reversibility with an Alloying Functional Layer in Anode-free Lithium Metal Batteries," *Nature Communications* 16 (2025): 7216.

159. Y. Hu, Z. Chen, Y. Wang, et al., "Review of Thin Lithium Metal Battery Anode Fabrication–Microstructure–Electrochemistry Relations," *Advanced Materials* (2025): 11817.

160. C. Zu, J. Li, B. Cai, et al., "Separators with Reactive Metal Oxide Coatings for Dendrite-free Lithium Metal Anodes," *Journal of Power Sources* 555 (2023): 232336.

161. W. Tang, T. Zhao, K. Wang, et al., "Dendrite-free Lithium Metal Batteries Enabled by Coordination Chemistry in Polymer-ceramic Modified Separators," *Advanced Functional Materials* 34 (2024): 2314045.

162. S. Gao, Y. Pan, B. Li, et al., "Ultra-Stretchable, Ionic Conducting, Pressure-Sensitive Adhesive with Dual Role for Stable Li-Metal Batteries," *Advanced Functional Materials* 33 (2023): 2210543.

163. G. Yu, Y. Cui, S. Lin, et al., "Ultrathin Composite Separator Based on Lithiated COF Nanosheet for High Stability Lithium Metal Batteries," *Advanced Functional Materials* 34 (2024): 2314935.

164. K. Wang, T. Zhao, R. Lv, et al., "Lithium Metal Batteries Enabled by Ion Flux-Regulating Coating on Separator," *Advanced Functional Materials* 35 (2025): 08164.

165. Z. Wang, H. Xu, K. Liu, et al., "Separator Engineering Regulating Reversible Li Electrodeposition Enabled by Lithiophilic Polyimide@ Ag Coating Layer for Dendrite-Free Lithium Metal Batteries," *Small* 21 (2025): 2504870.